Atmos. Meas. Tech. Discuss., doi:10.5194/amt-2016-244, 2016
Manuscript under review for journal Atmos. Meas. Tech.
Published: 15 August 2016

Atmospheric Measurement Techniques Discussions

Radiative characteristics of aerosol under smoke mist conditions in Siberia during summer 2012

Tatiana B. Zhuravleva[1], Dmitriy M. Kabanov[1], Ilmir M. Nasrtdinov[1], Tatiana V. Russkova[1], Sergey M. Sakerin[1], Alexander Smirnov[2,3] and Brent N. Holben[3]

[1]V.E. Zuev Institute of Atmospheric Optics SB RAS, Tomsk, Russia
[2]Science, Systems and Applications, Inc., Lanham, MD, USA
[3]NASA Goddard Space Flight Center, Greenbelt, MD, USA

Correspondence to: Tatiana Zhuravleva (ztb@iao.ru)

Abstract. Microphysical and optical properties of aerosol were studied during mega-fire event in summer 2012 over Siberia using ground-based measurements of spectral solar radiation at AERONET site in Tomsk and satellite observations. The data were analyzed using multiyear (2003-2013) measurements of aerosol characteristics under background conditions and for less intense fires, differing in burning biomass type, stage of fire, remoteness from observation site, etc. ("ordinary fires"). In June – August 2012, the average aerosol optical depth (AOD, 500 nm) had been 0.95±0.86, about a factor of 6 larger than background values (0.16±0.08), and a factor of 2.5 larger than in "ordinary smokes. The AOD values were extremely high on July 24-28 and reached 3-5. Comparison with satellite observations showed that ground-based measurements in the region of Tomsk not only reflect the local AOD features, but also are characteristic for the territory of the Western Siberia as a whole. Single scattering albedo (SSA, 440 nm) in this period ranged from 0.91 to 0.99 with the average of ~0.96 in the entire wavelength range of 440-1020 nm. The increase in absorptance of aerosol particles (SSA(440 nm)=0,92) and decrease in SSA with wavelength, observed in "ordinary smokes", agree with the data of multiyear observations in analogous situations in boreal zone of USA and Canada. Volume aerosol size distribution in smoke mist and ordinary smokes had bimodal character with significant prevalence of fine mode particles, but in summer 2012 the mean median radius and the width of the fine mode distribution somewhat increased. In contrast to data of multiyear observations, in summer 2012 an increase in the volume concentration and median radius of the coarse mode was observed with the growing AOD.

The calculations of the "average" radiative effects of smoke and background aerosol are presented. As compared to background conditions and "ordinary smokes", under the conditions of smoke mist the cooling effect of aerosol considerably intensifies: direct radiative effects (DRE) at the bottom (BOA) and at the top of the atmosphere (TOA) are -13, -35, and - 60 W m^{-2} and -5, -14, and -35 W m^{-2} respectively. The maximal values of DRE were observed on July 27 (AOD(500 nm)=3.5), when DRE(BOA) reached -180 W m^{-2}, while DRE(TOA) and DRE of the atmosphere were -80 W m^{-2}.

Atmos. Meas. Tech. Discuss., doi:10.5194/amt-2016-244, 2016
Manuscript under review for journal Atmos. Meas. Tech.
Published: 15 August 2016

Atmospheric Measurement Techniques Discussions

Key words: Sun-sky radiometer, AERONET, smoke mist in Siberia 2012, optical and microphysical properties of aerosol particles, diurnally radiative effects of smoke and background aerosol

1 Introduction

Massive forest and peat fires are the strongest source of aerosol-gas emissions on the territory of boreal zone of the Northern Eurasia. In addition to anthropogenic factor, the biomass ignition is favored by dangerous consequences of the global climate warming, manifesting in the form of strong temperature, circulation, and hydrologic anomalies (Groisman et al., 2007). In view of enormous stretches of boreal zone, fires occur in some or another region of this vast territory almost every year and influence strongly the radiation budget, air quality, human health, biological diversity, glaciology, etc. To understand the effects of biomass burning on the atmosphere, the physical, chemical and optical properties of smoke particles, it needs to be studied and parameterized with reliable uncertainties.

Since 1990s, a large amount of information on characteristics of carbonaceous particles based on in situ measurements and remote sensing using the ground-, aircraft- and satellite-based instruments has been accumulated in hundreds of manuscripts. However, even with the availability of such a volume of data, the determination of key parameters for estimating atmospheric effects of biomass burning is not straightforward, primarily because the smoke properties strongly depend on the set of a variety of reasons, the main of which are the type of biomass, the stage of fire, meteorological conditions at the fire site and on the territory of the dispersal of smoke plumes, age of smoke, etc. (see, e.g., the reviews Dubovik et al., 2002; Reid et al., 2005, 2005a; Bond and Bergstrom, 2006; Moosmu¨ller et al., 2009; Giles et al., 2012; Sayer et al., 2014; Nikonovas et al., 2015 and bibliography therein). Another problem is that specific features of individual fires may strongly differ from the ensemble smoke hazes that are a result of some averaging procedures of characteristics of numerous fires. This aspect is crucial for studying the radiation effects of aerosol because, in the framework of regional and global climate models, the most important issue is the development of model representations concerning the aged smoke that dominates regional hazes and affects climate.

A stable anticyclone had formed in summer 2012 in Siberian region under the conditions of small-gradient high-pressure baric field (Polyakov et al., 2014), with consequences being that forest and peat fires burned in a few regions of Siberia and encompassed the territory from 1 to 10 million hectares, by different estimates. Optical and microphysical properties of near-ground aerosol and specific features of their vertical structure according to data of in situ measurements, as well as spatiotemporal evolution of aerosol optical depth and active fires according to results of satellite monitoring, are presented in (Gorchakov et al., 2014; Kozlov et al., 2014; Sklyadneva et al., 2015; Vinogradova et al., 2015; Panchenko et al., 2016). In our work, we discuss the columnar optical and microphysical aerosol characteristics, retrieved on the basis of ground-based photometric observations in Tomsk during the period of smoke mist in 2012. The second aim is to compare these results with data of multiyear photometric measurements and satellite observations over the territory of the Western Siberia under the different atmospheric conditions.

Atmos. Meas. Tech. Discuss., doi:10.5194/amt-2016-244, 2016
Manuscript under review for journal Atmos. Meas. Tech.
Published: 15 August 2016

Atmospheric Measurement Techniques Discussions

2 Instrumentation, Sites, and Methods

2.1 Ground-based measurements

The measurements, presented in this paper, were made with CIMEL Electronique CE 318 sun-sky radiometer that is a part of AErosol RObotic NETwork (AERONET, (Holben et al., 1998)). These measurements were performed in eastern suburb of Tomsk ("Tomsk": 56.48°N; 85.05°E) in period of 2003-2010; and since 2011, CE 318 has been operated at "Fonovaya" observatory located 60 km away from the city ("Tomsk-22": 56.42ºN; 84.07ºE).

Direct Sun measurements are made in the spectral channels centered at 340, 380, 440, 500, 675, 870, 940 and 1020 nm (bandwidth: 10 nm at full width at half maximum). These solar extinction data are then used to compute aerosol optical depth (AOD, τ_λ) at each wavelength λ except 940 nm, which is used to retrieve total columnar content of water vapor (W). The spectral aerosol optical depth data have been screened for clouds following the methodology of Smirnov et al. (2000). In addition to direct Sun, radiation measurements in solar almucantar are made in four channels of CE 318: 440, 675, 870, and 1020 nm. These data and the inverse automated algorithm of Dubovik and King (2000) (version 1) with enhancements (version 2, Holben et al., 2006) were used to retrieve other aerosol characteristics: volume particle size distribution function $dV/d\ln r\left(\mu\text{m}^3\ \mu\text{m}^{-2}\right)$, scattering phase function, asymmetry factor g_λ, complex refractive index ($n_\lambda - \kappa_\lambda \times i$), and single scattering albedo ω_λ.

Dubovik et al. (2000a) presented uncertainty of retrieval estimates for volume size distribution, refractive index, and single scattering albedo (SSA). For Level 2 data at moderate aerosol loading (τ_{440} ~0.4) uncertainties for such retrievals are: 10-35% for the binned size distribution in the intermediate particle size range ($0.1 \le r \le 7\,\mu\text{m}$); 0.04 and 30-50% for the real and imaginary parts of the refractive index; and 0.03 for single scattering albedo. For typical biomass burning models (Dubovik et al., 2002) these uncertainties were propagated onto the other size distribution parameters (Sayer et al., 2014): the volume mean radius r_v and standard deviation σ of fine (f) and coarse (c) modes are retrieved with errors 0.01 μm for r_v^{f}, 0.2 μm for r_v^{c}, and 0.06 for σ^{f} and σ^{c}. This led to uncertainties of ~0.015–0.04 in the asymmetry factor (AF) of fine aerosol mode (larger uncertainties at longer wavelengths) and ~0.01 in the coarse mode aerosol (smaller uncertainties at longer wavelengths).

An original approach, relying upon ground-based spectral measurements of AOD and radiance phase functions, was also used in addition to the algorithm of Dubovik and King (2000) to solve the inverse problem. The first version of the algorithm, namely, Sun-Sky Measurements for Aerosol ReTrieval (SSMART 1.1 software package), was implemented under the assumption of (a) the sphericity of aerosol particles and (b) the independence of the complex refractive index on the wavelength and particle size (Bedareva et al., 2013a). An improved version of the algorithm (SSMART 1.2), in which the inverse light scattering problem was solved using the model of a mixture of randomly oriented polydisperse spheroids, was suggested by Bedareva et al.

Atmos. Meas. Tech. Discuss., doi:10.5194/amt-2016-244, 2016
Manuscript under review for journal Atmos. Meas. Tech.
Published: 15 August 2016

Atmospheric Measurement Techniques Discussions

(2014). In both versions, the aerosol optical characteristics are derived in two ways: directly from the spectral Sun-sky radiometer measurements (Way 1) and through the calculation based on the retrieved particle size distribution and complex refractive index (Way 2). On the basis of closed numerical experiments, the accuracy of aerosol retrievals was investigated in error-free conditions and in the presence of measurement errors. The SSMART algorithm was tested as applied to conditions of moderate and increased aerosol turbidity of the atmosphere at Tomsk and Dakar (14 N, 16 W) AERONET sites. It was found that the SSMART and AERONET codes give the consistent estimates of aerosol properties within their retrieval uncertainties (Bedareva et al., 2013ab, 2014).

Measured aerosol optical depth and computed retrieval products were used to derive additional aerosol properties. Spectral dependence of AOD is traditionally described by the empirical Ångström formula

$$\tau_{\lambda} = \beta\lambda^{-\alpha}. \quad (1)$$

The absorption AOD (AAOD) is calculated for each wavelength using the following equation (Giles et al., 2012)

$$\tau_{abs,\lambda} = \tau_{\lambda} \times \left[1 - \omega_{\lambda}\right] \quad (2)$$

and, similar to Eq. (1), it can be represented as

$$\tau_{abs,\lambda} = \beta_{abs}\lambda^{-\alpha_{abs}}. \quad (3)$$

Analyzing the radiative characteristics of aerosol in the period of 2012 smoke mist, we additionally employed data of multiyear AOD observations at “Tomsk” and “Tomsk-22” sites, obtained from April to October in 2003-2011 and in 2013. Using the method of Kabanov and Sakerin (2006), the total dataset was divided into two subsets: 1) “background” (usual) conditions (998 days); and 2) “ordinary” smoke situations (81 days). By the “ordinary” smokes we mean smoke situations from yearly observed Siberian biomass burning of different types (forest and peat fires, springtime vegetation burning, smokes from remote sources), which were shorter lasting and less severe as compared to 2012 smoke mist. Simultaneous measurements at these sites revealed no statistically significant AOD differences in the warm period of the year (Sakerin et al., 2010); therefore, merging of data, obtained at the neighboring sites (“Tomsk” and “Tomsk-22”), can be regarded as correct.

Smaller data volume had gone into comparative analysis of aerosol optical and microphysical characteristics obtained from the inverse procedure. The number of retrievals of total set of characteristics, including refractive index, single scattering albedo, volume size distribution function, and scattering phase function (Level 2, $\tau_{440} > 0.4$), had been 65 in the period of smoke mist (June 15 – August 10, 2012), and 140 under the conditions of “ordinary” smokes (April – October 2003-2011, 2013). Out of 140 “ordinary” smoke situations, maximal number of almucantar retrievals had been 39 (2004), 23 (2006), and 22 (2013). In these data, results obtained in May 2004 deserve a special attention. Dry and warm weather, predominating in Novosibirsk and Tomsk regions (with air temperatures exceeding 30ºC on separate days) led to numerous forest fires, provoked by burning of last year’s vegetation and bonfires, left unextinguished by fishers and hunters. The number of retrieved aerosol characteristics varied from 1 (2005) to 15 (2008) for remaining period of multiyear observations.

Atmos. Meas. Tech. Discuss., doi:10.5194/amt-2016-244, 2016
Manuscript under review for journal Atmos. Meas. Tech.
Published: 15 August 2016

Atmospheric Measurement Techniques Discussions

145
146 **2.1 Satellite data**
147
148 AOD observations at 550 nm (collection 6, http://giovanni.sci.gsfc.nasa.gov/giovanni/) and Aerosol Small
149 Mode Fraction (collection 5, http://gdata1.sci.gsfc.nasa.gov/daac-
150 bin/G3/gui.cgi?instance_id=MODIS_DAILY_L3, valid at time of manuscript preparation) from MODIS
151 instruments were used. These MODIS products (TERRA and AQUA platforms, Level 3 data, i.e., daily
152 averaged within the grid cells 1º×1º) were obtained using the algorithm of Levy et al. (2010).
153
154 **3 General characteristics of the large-scale smoke pollution in the summer of 2012**
155
156 In this section, we present the general characteristics of smoke situation in 2012 on the territory of Tomsk
157 region.
158
159 **3.1 Weather-climate features**
160
161 In summer 2012, a stable anticyclone had formed over the territory of Siberia under the conditions of
162 small-gradient high-pressure baric field (Polyakov et al., 2014), the consequences being substantial changes in
163 climatically significant characteristics and, primarily, an appreciable increase in air temperature and a decrease
164 in precipitation. Data of observations at "Tomsk" meteorological station (WMO_ID=29430, http://rp5.ru)
165 indicate that monthly mean temperature in July was maximal over last decade, while precipitation amount was
166 close to a minimum (Figure 1). On the whole, positive anomalies of temperature reached 1.3-7.2ºC in June-
167 July on the territory of Tomsk region (~56-61ºN; 75-88ºE), and precipitation amount was 20-30% of climatic
168 norm. Selyaninov hydrothermal wetting coefficient was also used as a characteristic of wetting (drought)
169 regime (see, e.g., (Polyakov et al., 2014)); it is defined as the ratio of precipitation total for period no shorter
170 than one month to the sum of temperatures for the same period, decreased by a factor of ten. Polyakov et al.
171 (2014) showed that, over the last 70 years, the atmospheric droughts on the territory of Tomsk region were
172 longer than one month in nine summer seasons (the hydrothermal wetting coefficient varied from 0.6 to 1.4),
173 with the summer of 2012 being the driest one.
174 These conditions had led to extensive forest fires in the Western and Eastern Siberia (Figure 2),
175 accompanied by considerable pollution of the atmosphere by combustion products (smoke particles, carbon
176 and nitrogen oxides, etc.). Ground-based observations in Tomsk indicate that, in period of maximal smoke
177 pollution on July 25-28, 2012, the aerosol number concentration had been 3000-8500 cm^{-3} (particle size 0.4-15
178 μm), exceeding the background values by about a factor of 20, while carbon monoxide concentrations reached
179 7.7 ppm (Sklyadneva et al., 2015). Results of satellite (AIRS/TERRA) monitoring indicate that the July-
180 average total CO content over the territory of Tomsk region in 2012 increased by approximately 40% (Fig. 1)
181 as compared to 2005-2015 (except 2012).

Atmos. Meas. Tech. Discuss., doi:10.5194/amt-2016-244, 2016
Manuscript under review for journal Atmos. Meas. Tech.
Published: 15 August 2016

Atmospheric Measurement Techniques Discussions

Anticyclone over the territory of the Western Siberia persisted for almost two months (second half of June – first decade of August), similar to anomalous situations observed over the European territory of Russia in 1972 and 2010 (Shakina and Ivanova, 2010). At the end of first decade of August, the blocking cyclone started to break, heat rapidly weakened, and air temperature returned to within the climatic norm at all meteorological stations of Tomsk region (Polyakov et al., 2014).

3.2 Aerosol radiation characteristics

3.2.1. Ground-based observations

Figure 3abc shows the time variations in daily average values of AOD, single scattering albedo ω_{440}, and asymmetry factor g_{440} in the summer period of 2012.

The AOD data indicate that there are two waves of high atmospheric smoke turbidities: from June 17 to July 5, and from July 19 to August 6. Maximal AOD values (500 nm), reaching 3-5, were observed on July 3-6 and July 25-29.

The single scattering albedos did not go out of the interval $0.93 \le \omega_{440} \le 0.99$ in almost all cases. The asymmetry factor g_{440} varied from 0.66 to 0.74, i.e., in the same range as multiyear average values on the territory of Siberia (Sakerin et al., 2009, 2012, 2014). From results presented here it also follows that, on those days when SSA and AF were retrieved by two methods, the SSMART and AERONET codes gave consistent estimates of aerosol properties within their retrieval uncertainties.

Arrival of smoke plumes was also accompanied by a substantial increase in the mass concentrations of black carbon (M_{BC}) and aerosol (M_a) in the near-ground atmospheric layer. Kozlov et al. (2014) showed that the average values of these characteristics at "Fonovaya" observatory in the period from June 17 to August 4 varied in the ranges M_{BC}=1.9-10.3 μg m^{-3} and M_a=103-425 μg m^{-3} given the background levels of ~0.45 and ~20 μg m^{-3} respectively for August 10-31. Similar to AOD, the maximal concentrations of M_{BC} and M_a were observed in the period of July 25-29.

The examples of daily average aerosol volume size distribution $dV/d\ln r$ for moderate to high AOD values are presented in Figure 3d. A noticeable salient feature of the $dV/d\ln r$ distribution is the increase in the modal radius and in the width of the mode of finely dispersed fraction during extreme turbidity on July 28 as compared to periods on June 27 and July 14, when AOD was much lower.

A consequence of anomalously high atmospheric turbidities had been substantial changes in solar radiation reaching the earth's surface. Figure 4 illustrates the daytime behavior of direct and diffuse radiative fluxes, measured with MS-53 pyrheliometer and MS-802 pyranometer (0.305-2.8 μm) under usual (background) conditions on July 24, 2011 (τ_{500} = 0.07) and in the highly turbid atmosphere on July 28, 2012 (τ_{500} = 2.14). Under the influence of smoke plume, there was a two- to four-fold decrease in direct radiation, which was partially compensated for by approximately equal increase in diffuse radiation. The diffuse

Atmos. Meas. Tech. Discuss., doi:10.5194/amt-2016-244, 2016
Manuscript under review for journal Atmos. Meas. Tech.
Published: 15 August 2016

Atmospheric Measurement Techniques Discussions

radiation was considerably (a factor of ~1.8) larger than the direct radiation throughout the day (July 28, 2012).

3.2.2 Satellite observations

The spatial distributions of AOD at 550 nm and Aerosol Small Mode Fraction ($\eta_{550} = \tau^{f}_{550} / \tau_{550}$) over Western and partially Eastern Siberia (60º-100ºN, 52º-70ºE), averaged over the period of June 15 – August 10, 2012, are presented in Figure 5. These data show that the territory of the Tomsk region in this period was subjected to intensive influence of large-scale smoke pollution and characterized by high values of AOD and content of fine aerosol fraction: $\tau_{550} > 0.9$; $\eta_{550} > 0.7$.

4. Discussion of results

4.1 Temporal and Spectral Variability of Aerosol Optical Depth

4.1.1. Ground-based data

Analysis of multiyear AOD variations in a few regions of Russia according to data of photometric observations showed that, after eruption products of Pinatubo volcano had sunk out of the stratosphere, the interannual AOD variations were small and no statistically significant trend was observed in the past two decades (Sakerin et al., 2009, 2012; Sakerin and Kabanov, 2015). For instance, the annually average AOD values (500 nm) in Tomsk during the period of 2003-2015 (except in 2012) varied from 0.13 to 0.21 (Figure 6a).

Under the influence of massive forest fires in Siberia during summer 2012, the annual AOD value had exceeded the multiyear norm by almost a factor of two and became the highest over the entire period of photometric observations in Tomsk (since 1992) (Sakerin and Kabanov, 2015). Average summertime AOD values changed even stronger: in particular, the average value τ_{500} in July had increased by a factor of 4.5 as compared to multiyear data (Figure 6b). Even if we omit anomalously high turbidities ($\tau_{500} > 1$), which may be partly due to clouds invisible through haze, the average AOD values in summer months of 2012 go out of the corridor defined by standard deviations (SDs).

More detailed characteristics of atmospheric AOD for three wavelengths in UV, visible, near IR ranges during the smoke mist in comparison with the multiyear average data for July are presented in Table 1. Also given are the average characteristics for various situations of “ordinary” smokes, which are observed every year in Siberia in warm period. The comparison showed (see also Figure 6c) that AOD during smoke mist exceeds the background values by a factor of 5.5-6 in the entire spectral range. In absolute value, AOD increased stronger in shortwave part of spectrum, i.e., due to finely dispersed aerosol. The slight increase in Ångström exponent α, which depends on the interrelation between contributions of fine and coarse aerosols to

Atmos. Meas. Tech. Discuss., doi:10.5194/amt-2016-244, 2016
Manuscript under review for journal Atmos. Meas. Tech.
Published: 15 August 2016

Atmospheric Measurement Techniques Discussions

AOD, also indicates that small particles predominate in smoke aerosol. Despite the temperature, aerosol, and other anomalies, the total water vapor content of the atmosphere in the period of smoke mist differed little from the multiyear norm.

Average AOD characteristics in "ordinary" smokes incorporate data for fires of different types and distances from the region of measurements and, as such, occupy an intermediate position between background conditions and smoke mist. Independent of their intensity (mist or "ordinary" smokes), a common feature of all smokes is an identical exponent α, which characterizes higher content of fine aerosol.

It is noteworthy that the multiyear average values of α and AOD in the near-IR range, calculated for background conditions and total dataset, differ little (see columns 2 and 3 in Table 1), primarily because of relatively small number (about 8%) of smoke situations in the total dataset.

Under the assumption that aerosol size distributions are bimodal, O'Neil et al. (2001, 2003) have developed a spectral deconvolution algorithm (SDA) to infer the component fine and coarse mode optical depth from spectral dependence of AOD. In June-August 2012, the coarse mode τ_{500}^{c} is less than fine mode τ_{500}^{f} and is typically low (only 3 days show that τ_{500}^{c}~0.2), whereas τ_{500}^{f} is high and exhibits very large day-to-day variability (Figure 7a). The parameter η_{500}, which characterizes the contribution of fine fraction to AOD at 500 nm, exceeded 0.7 and approached 0.9 at $\tau_{500} \geq 0.6$ (Figure 7b). These results are consistent with earlier published data, according to which content of finely dispersed aerosol predominately increases during vegetation burning in the absence of any other significant sources (Reid et al., 2005a; Eck et al., 2009; Giles et al., 2012).

4.1.2 Analysis of satellite observations

Analysis of spatiotemporal AOD variations was confined to the consideration of the central part of the Western Siberia. A salient feature of this territory is a uniform landscape (without mountainous terrain) and the absence of large sources of anthropogenic pollution. Under usual conditions, the AOD values, retrieved from satellite observations, are characterized by small (background) values and by quite a uniform spatial distribution (Zhuravleva et al., 2009a; Sakerin et al., 2012).

Since the formation and evolution of smoke plumes are strongly affected by large-scale atmospheric dynamics, spatial distributions of AOD may substantially change from one day to another. The main specific features of variations can be identified through analysis of AOD fields, averaged for a few 5-day periods, selected by taking into account the ground-based observations (Fig. 3a): on June 6-10 there were background conditions (before beginning of forest fires); on July 1-5 and July 24-28 there were maximal smoke turbidities; and on July 10-14 there were relatively low AOD values observed between two turbidity maxima. Hereinafter, for calculations of the AOD values averaged over the selected time interval (5 days) we used the daily satellite product.

Spatial AOD distributions, presented in Figure 8, show that the "Tomsk-22" observation site was either at the center (Fig. 8b) or on the periphery of smoke plumes (Fig. 8a) in different periods of time. The periods

Atmos. Meas. Tech. Discuss., doi:10.5194/amt-2016-244, 2016
Manuscript under review for journal Atmos. Meas. Tech.
Published: 15 August 2016

Atmospheric Measurement Techniques Discussions

of small turbidities of the atmosphere (on June 6-10 and July 10-14) were characterized by quite a uniform AOD distribution, and the largest spatial inhomogeneities and values $\tau_{550} > 1$ were observed over the central part of the Western Siberia on July 24-28 (Fig. 8 and Table 2).

The statistical characteristics in Table 2 were calculated using measurements from AQUA and TERRA platforms (MODIS collection 6, http://giovanni.sci.gsfc.nasa.gov/giovanni). These data suggest that, for three out of four periods considered here, the average AOD values at "Tomsk-22" site are close to spatiotemporal averages on the entire territory of the Western Siberia: the difference between satellite and ground-based data is much less than standard deviations, except in period of July 24-28, when the average AOD at "Tomsk-22" site had been $\tau_{550} = 2.74$ and exceeded the average value for the Western Siberia (MODIS) $\tau_{550} = 1.06$. At the same time, the satellite data in the ($1^o \times 1^o$) region of "Tomsk-22" site well agree with results of photometric observations. Thus, the results of ground-based measurements in the region of "Tomsk-22" can be considered to reflect not only the local AOD features, but also the regularities of variations for the entire territory of the Western Siberia.

4.2. Retrieval results

We will compare the retrievals of aerosol optical and microphysical characteristics under the conditions of smoke mist in 2012 against the average data for ordinary smokes (Table 3). Since the AOD dependence of C_v and r_v for fine and coarse aerosol modes has previously been noted for a wide variety of aerosol types (including biomass burning aerosol (Dubovik et al., 2002; Sayer et al., 2014)), Table 3 also presents the resulting linear regression relationships between the pairs $(C_v^{f(c)}, \tau_{440})$ and $(r_v^{f(c)}, \tau_{440})$, as well as the corresponding linear correlation coefficients *R*.

4.2.1 Volume size distributions

During the period of smoke mist in 2012, the average values of volume median radii for finely and coarsely dispersed fractions were $r_v^f = 0.18$ μm and $r_v^c = 3.3$ μm, a little larger than these characteristics for ordinary smokes, equaling 0.16 μm and 2.9 μm respectively (Table 3). The r_v^f value, in both cases, was in the range of values, obtained for biomass burning in other regions of the globe (Reid et al., 2005, 2005a; Eck et al., 2009; Chubarova et al., 2012), as well as in the range of measurements for aged smoke, performed using Optical Particle Counter (0.1 – 3 μm) and Differential Mobility Particle Sizer (0.01 - 0.6 μm) in boreal zones of Europe and North America (Reid et al., 2005). Like in Siberia, the wider size distribution of fine particles than for ordinary smokes (Table 3; Fig. 3d) was also noted by other authors for severe fires in boreal zone of Alaska (Bonanza Creek, 2004-2005, Eck et al., 2009).

The noteworthy salient features of finely dispersed fraction during summer 2012 are as follows. The contribution of finely dispersed fraction to the total volume (C_v^f / C_v^t), on the average, increased to

Atmos. Meas. Tech. Discuss., doi:10.5194/amt-2016-244, 2016
Manuscript under review for journal Atmos. Meas. Tech.
Published: 15 August 2016

Atmospheric Measurement Techniques Discussions

328 0.8 ± 0.065 as compared to value 0.65 ± 0.21 according to multiyear observations. Volume concentrations and
329 volume median radii of the fine mode are plotted in Figure 9a as functions of AOD at 440 nm. This figure
330 shows that there is general increase in volume concentrations C_v^{f} as τ_{440} increases (Fig. 9a). The median
331 radius of the fine mode increased from about 0.15 to 0.22 μm as τ_{440} changed from 0.4 to 1.5 and larger (Fig.
332 9b). The smoke particles have large radii, and r_v^{f} and τ_{440} are closely correlated, possibly because of high
333 concentration of aerosol, which leads to greater coagulation, condensation, and gas-to-particle conversion
334 (Reid et al., 1998, 2005; Eck et al., 2009). From this figure it also follows that the interrelation between
335 median radius of finely dispersed fraction and AOD at 440 nm in ordinary smokes is much less pronounced,
336 primarily because of the variety of properties biomass burning aerosol combined in this dataset. For instance,
337 in May 2004, the median radius was relatively small ($r_v^{\mathrm{f}} \sim 0.14$ μm) and did not practically change with
338 varying τ_{440}. Most probably, this was because burning of last year's vegetation was one of the sources of
339 smoke particles in this period of time. (An analogous feature was also observed during African savanna fires
340 (Dubovik et al., 2002)).
341 In contrast to data of multiyear observations, in summer 2012 an increase in the volume concentration
342 and median radius of the coarse mode was observed with the growing AOD. Most probably, soil particles,
343 being suspended by saltation of surface dust driven by fire generated winds, were also present during this
344 period of time in the composition of coarse mode in addition to carbon aggregates.
345 Results of retrieval of disperse composition of finely dispersed aerosol in the atmospheric column agree
346 with measurements in near-ground layer (Kozlov et al., 2014). Data of spectral-polarization nephelometric
347 measurements were used to show that the volume median radius of the fine mode under the conditions of weak
348 turbidity of the atmosphere (July 10–13, 2012) had increased from 0.1 μm to 0.4-0.5 μm when smoke plumes
349 intruded to the region of observations (July 25–29, 2012).
350
351 **4.2.2 Refractive index**
352
353 Average values of the real and imaginary parts of refractive index under the conditions of smoke mist and
354 ordinary smokes are presented in Table 3. In ordinary smokes, the imaginary part of refractive index κ_λ
355 changes weakly with the increasing wavelength and is approximately 0.01. However, the imaginary refractive
356 index in the Tomsk smoke mist shows low values and relatively large decrease in κ_λ as the wavelength grows
357 from 440 to 675 nm. The κ_λ variations in the wavelength interval of 675-1020 nm are not as strong.
358 The quantitative differences and specific features of spectral dependence of the imaginary refractive
359 indices stem from different properties of atmospheric carbonaceous particles, i.e., black carbon (BC) and
360 organic aerosol (OA). Recent studies showed that OA components can contribute substantially to light
361 absorption. In contrast to BC, which absorbs light throughout the UV-visible spectrum, such an OA
362 component as "brown carbon" (BrC) absorbs mostly in the ultraviolet wavelength and less significantly in the
363 visible spectral range (Kirchstetter et al., 2004; Bergstrom et al., 2007; Chen and Bond, 2010; Zhong and

Atmos. Meas. Tech. Discuss., doi:10.5194/amt-2016-244, 2016
Manuscript under review for journal Atmos. Meas. Tech.
Published: 15 August 2016

Atmospheric Measurement Techniques Discussions

Jang, 2014). The majority of BrC is emitted to the atmosphere through low temperature, incomplete combustion of biomass, bio- and fossil fuel (Bond, 2001; Kirchstetter et al., 2004; Bergstrom et al., 2007; Lewis et al., 2008; Chen and Bond, 2010; Zhong and Jang, 2014).

The absorption efficiency and spectral dependence vary depending on the type of BrC origin. Lu et al. (2015) reviewed available measurements (laboratory and field observations) of light-absorbing primary organic aerosols, and quantify the wavelength-dependent imaginary refractive indices (κ_{OA}) for the bulk primary OA emitted from biomass/biofuel, lignite, propane and oil combustion sources. Based on generalized information, they suggested to parameterize κ_{OA} of biomass/biofuel combustion sources as a function of BC-to-OA ratio. Analysis of imaginary refractive indices showed the stronger wavelength-dependent κ_{OA} for lower BC-to-OA ratio conditions (smoldering combustion), while the greater κ_{OA} values at λ>350 nm are observed for higher BC-to-OA ratio (flaming combustion).

These results allow us to hypothesize that the reason for the κ_λ decrease in the interval of 440-675 nm during summer 2012 may be due to the contribution of compounds absorbing radiation in UV wavelength region ("brown" carbon). To confirm this hypothesis, we considered OMI observations of the Ultraviolet Aerosol Index (UVAI), the value of which is sensitive to aerosol absorption in the ultraviolet wavelength region (Torres et al., 1998; Jethva and Torres, 2011; Hammer et al., 2016)]. Satellite data indicate that UVAI values were quite high in the period of smoke mist, and exceeded 4-5 on individual days, thus explaining the above-mentioned κ_λ decrease in going from UV to visible spectral region (Figure 10).

The relatively constant imaginary refractive index in ordinary smokes owes to averaging over many situations, differing, in particular, in the type of burning biomass (peat, forest, grass). For instance, in May 2004, when the characteristics of smoke aerosol were quite homogeneous, the average spectral behavior of κ_λ was weakly manifested, with $\kappa_\lambda \approx 0.013$ in the interval of 440-1020 nm. At the same time, the UVAI value did not exceed 1.2 (http://giovanni.sci.gsfc.nasa.gov/giovanni/), suggesting that BC was seemingly the main absorbing substance in this period of time.

4.2.3 Single scattering albedo

Detailed analysis of spectral SSA in 2012 has revealed two types of dependence: monotonically decreasing and monotonically increasing ω_λ with the growing wavelength (Figure 11).

The main group of SSA data (45 cases out of 65) is characterized by a weakly decreasing spectral dependence: the range of the differences $\Delta\omega_\lambda = \omega_{440} - \omega_{1020}$ did not exceed 0.03 (Fig. 11a). Practically all set of retrieved SSA of this type lies between the curves 2 ($\omega_{440} = 0.926$) and 3 ($\omega_{440} = 0.996$). In other cases, the ω_λ decrease with the growing wavelength is larger, but does not exceed 0.06 (curve 4, Fig. 11a). We note that the values of the imaginary part of refractive index are ~0.006 for this subset of data.

Atmos. Meas. Tech. Discuss., doi:10.5194/amt-2016-244, 2016
Manuscript under review for journal Atmos. Meas. Tech.
Published: 15 August 2016

Atmospheric Measurement Techniques Discussions

In a few (14 out of 65) situations with high atmospheric turbidities ($\tau_{440} > 0.9$), there was an increase in SSA with the growing wavelength (curve 1 in Fig. 11a). The monotonic increase in ω_λ agrees with decrease in κ_λ (on the average, from 0.01 at 440 nm to ~0.006 at 675 nm), presumably due to additional absorption of "brown" carbon in the UV wavelength region.

On the whole, the 2012 smoke mist was characterized by weak spectral variations in SSA, the average being ~0.96, consistent with previous results in other regions of Eurasian boreal zone: in Moscow (2002 and 2010) and Alaska (2004-2005), where the smoldering phase prevailed over the flaming fire phase (Eck et al., 2009; Chubarova et al., 2011; Sayer et al., 2014). The relatively constant spectral single scattering albedo of smoke mist in 2012 may be also partly due to growth of aerosol particle sizes (Subsect. 4.2.1, Table 3; see also Eck et al., 2009).

The SSA retrievals in atmospheric column satisfactorily agree with data in the ground-layer (Kozlov et al., 2014), according to which the single scattering albedos in the visible range (λ=510 nm) were in the interval of 0.95-0.98. At the same time, the imaginary and real parts of the complex refractive index of dry base of substance varied in the ranges of 0.01-0.02 and 1.36-1.47 respectively.

Overwhelming majority of results of individual retrievals in "ordinary" smokes also showed a monotonic SSA decrease with the increasing wavelength, with the opposite dependence being observed in only 6 cases out of 140. However, in contrast to smoke mist, the spectral SSA behavior was stronger pronounced: $\Delta\omega_\lambda$ reached 0.06-0.18 in 18% of cases; $\Delta\omega_\lambda$ was 0.03-0.06 in 40% of cases, and $\Delta\omega_\lambda$ was less than 0.03 in 34% of cases.

The average single scattering albedos in "ordinary" smokes, presented in Fig. 11b, turned out to be about 0.02 lower than those observed in boreal forests of USA and Canada (Dubovik et al., 2002). These differences may be both due to methodic and physical factors. Methodic-type differences might stem from different methods for selecting the smoke situations. The specific features of the spectral dependence of SSA can also be explained by different combinations of the composition and age of smoke aerosol, which were recorded at AERONET observation sites. This is clearly illustrated by results obtained in May 2004 in Tomsk (Fig. 11b). Lower values and pronounced spectral variations of SSA (a decrease from 0.9 to 0.85) may be due to the last year's grass and agricultural vegetation combustion products, present in the smoke composition, as well as due to flaming phase of combustion which predominated in that period of time. (Close values and analogous spectral dependence of single scattering albedo were also noted in African savanna fires (Zambia), Dubovik et al., 2002, Sayer et al., 2014).

Aerosol absorption optical depth $\tau_{abs,\lambda}$ and absorption Ångström exponent α_{abs}, computed for the spectral interval of 440-870 nm (Sect. 2), were considered as other characteristics of absorbing properties of aerosol particles.

Data, presented in Fig. 11d, show that the average values of $\tau_{abs,\lambda}$ in the period of smoke mist were about a factor of 1.5-2 smaller than for "ordinary" smokes. In addition, there are differences in α_{abs}, which are 1.6±0.44 (smoke mist) and 1.2±0.5 (ordinary smoke) respectively.

Atmos. Meas. Tech. Discuss., doi:10.5194/amt-2016-244, 2016
Manuscript under review for journal Atmos. Meas. Tech.
Published: 15 August 2016

Atmospheric Measurement Techniques Discussions

The AAE values can be used as an indicator of aerosol composition (Andreae and Gelencsér, 2006; Russell et al., 2010; Schuster et al., 2016). The relatively low values α_{abs}~1 are typical for aerosol absorption largely dominated by black or light absorbing carbon, while larger values suggest absorption by different material organic carbon (Bergstrom et al., 2002, 2007; Kirchstetter et al., 2004; Lewis et al., 2008; Russell et al., 2010; Schuster et al., 2016). The α_{abs} increase in the 2012 fires may indicate that, on the average, smoke absorption possibly shifted from domination by black carbon in "ordinary" smokes to an increasing influence of absorption by other materials most likely organic carbon (see also Fig. 10).

In contrast to single scattering albedo, the spectral asymmetry factor differs insignificantly among the 2012 smoke mist, "ordinary" smokes, and May 2004 smokes (Table 3, Figure 11c).

5. Radiative effects of smoke aerosol

The radiative effects of smoke aerosol were accounted for by calculating the transmittance (*T*), albedo (*A*), and absorptance of the atmosphere (ABS_{ATM}) and underlying surface (ABS_{SUR}):

$$T = 100\% \times F_{BOA}^{\downarrow} / F_{TOA}^{\downarrow}, \quad A = 100\% \times F_{TOA}^{\uparrow} / F_{TOA}^{\downarrow}, \tag{4}$$

$$ABS_{ATM} = 100\% \times \left(F_{TOA}^{\text{net}} - F_{BOA}^{\text{net}}\right) / F_{TOA}^{\downarrow},$$

$$ABS_{SUR} = 100\% \times F_{BOA}^{\text{net}} / F_{TOA}^{\downarrow}.$$

Here, $F_{BOA(TOA)}^{\downarrow(\uparrow)}$ are broadband solar radiative fluxes in the interval of (0.2-5 μm), the symbols ↓(↑) are used to denote the downward and upward radiation at the top of the atmosphere (TOA) and bottom of the atmosphere (BOA). Radiative influxes F^{net} at different levels are calculated as follows

$$F_{BOA(TOA)}^{\text{net}} = F_{BOA(TOA)}^{\downarrow} - F_{BOA(TOA)}^{\uparrow} \tag{5}$$

The results of radiative flux simulation were used to calculate the direct radiative effect (DRE) at TOA and BOA and in atmospheric column:

$$\Phi_{TOA(BOA)} = F_{TOA(BOA)}^{\text{net},a} - F_{TOA(BOA)}^{\text{net},R}, \ \Phi_{ATM} = \Phi_{TOA} - \Phi_{BOA}, \tag{6}$$

where the superscripts "*a*" and "*R*" correspond to the calculations in aerosol-molecular atmosphere and in the aerosol–free atmosphere, with only molecular (Rayleigh) scattering and absorption taken into consideration. The negative and positive DRE values are associated with an aerosol cooling and warming, both at TOA and BOA. In addition to the proper DRE, we also considered the radiative effect efficiency

$$\Phi_{TOA(BOA)}^{e} = \Phi_{TOA(BOA)} / \tau_{550}, \ \Phi_{ATM}^{e} = \Phi_{ATM} / \tau_{550}, \tag{7}$$

which characterizes the rate at which the atmosphere is forced per unit of AOD at 550 nm at TOA and BOA. The Φ^{e} value depends on reflective properties of underlying surface, size distribution of aerosol particles, and their chemical composition; also, it depends on AOD, to some extent (due to the multiple scattering effects).

5.1 Model and input data

Atmos. Meas. Tech. Discuss., doi:10.5194/amt-2016-244, 2016
Manuscript under review for journal Atmos. Meas. Tech.
Published: 15 August 2016

Atmospheric Measurement Techniques Discussions

The broadband fluxes of the solar radiation in the molecular-aerosol plane-parallel atmosphere were calculated using the algorithm of the Monte Carlo method, which we developed earlier (Zhuravleva et al., 2009a). The radiative fluxes at a given atmospheric level z are represented as a sum of fluxes in separate wavelength intervals:

$$F^{\downarrow(\uparrow)}(z) = \sum_{i=1}^{M} F_i^{\downarrow(\uparrow)}(z), \quad (8)$$

where M =31 is the number of bands $\Delta\lambda = (\lambda_i, \lambda_{i+1})$, $i = 1,...M-1$, $\lambda_1 = 0.2$ μm, $\lambda_M = 5.0$ μm. Within each subinterval, the optical characteristics of aerosol and molecular scattering coefficient are assumed to be constant and equal to their values in the middle of subsinterval. The transmission function is approximated by a finite exponential series (k-distribution method). The algorithm intrinsically takes into account the multiple scattering, absorption by aerosol and molecular particles, as well as reflection of incident radiation from the underlying surface according to Lambert law. The comparisons showed that the numerical simulation results are in a satisfactory agreement with results of line-by-line calculations and data of field measurements (Tvorogov et al., 2008; Zhuravleva et al., 2009a, 2014).

The spectral AOD (340-1020 nm), the water vapor content, the column-integrated single scattering albedo, and the asymmetry parameter taken from AERONET were used as the main input parameters of the algorithm under the smoke conditions. In the interval of 440-1020 nm, the spectral values ω_λ and g_λ have been linearly interpolated from the values of SSA and AF retrieved at the four AERONET inversion wavelengths, while for $\lambda \le 440$ nm and $\lambda \ge 1020$ nm they have been considered constant, similar to Garsia et al.(2012) and Panchenko et al. (2012). Under the background conditions, Level-2.0 retrieval products for the single scattering albedo and asymmetry factor, obtained on the basis of standard AERONET algorithm, are not available due to low AOD values ($\tau_{550} = 0.13$ according to data of multiyear ground-based measurements under summer conditions, Sakerin et al., 2009; Sakerin and Kabanov, 2015). Therefore, OPAC model (averaged continental aerosol, relative air humidity is 70%, (Hess et al., 1998) was used to simulate the radiative characteristics under the conditions of the weakly turbid atmosphere.

As in (Panchenko et al., 2012), the aerosol optical depth was assumed to be constant outside the wavelength interval of 340-1020 nm: $\tau(\lambda \le 340\,nm) = \tau_{340}$, $\tau(\lambda \ge 1020\,nm) = \tau_{1020}$. Such an approach was chosen for the following reasons. The contribution of solar radiation, incoming at TOA in the interval of 200-340 nm, is about 3.5%; therefore, in the absence of measurements, the specified character of spectral dependence of AOD cannot influence significantly the simulation results. Based on the data of multiyear ground-based observations on the territory of Siberia, Sakerin and Kabanov (2007) showed that AOD hardly varies in the interval λ>1000 nm; therefore, we can assume that τ(λ>1000 nm)~ τ(λ~1000 nm).

The molecular absorption coefficients were calculated on the basis of HITRAN2008 database and MT_CKD v.2.4 continuum model (http://rtweb.aer.com/continuum_frame.html), using a regional model of temperature, pressure, and water vapor concentration profiles (Komarov and Lomakina, 2008), taking into account the absorption by all atmospheric gases, which was presented in the AFGL meteorological model

Atmos. Meas. Tech. Discuss., doi:10.5194/amt-2016-244, 2016
Manuscript under review for journal Atmos. Meas. Tech.
Published: 15 August 2016

Atmospheric Measurement Techniques Discussions

(Anderson et al., 1986). The profiles of ozone O_3 and carbon dioxide CO_2 were specified taking into consideration the data of multiyear observations, obtained on the territory of the Western Siberia during summer period: the total O_3 content was taken to be equal to 340 DU (according to data of TOMS satellite instrumentation, 2000-2010), and the CO_2 mixing ratio was taken to be equal to 380 ppm (according to data of aircraft sensing in 1997-2007 (Arshinov et al., 2009)).

It is well known that the surface albedo affects (primarily upward) radiative fluxes and may even cause DRE sign reversal (see, e.g., Zhuravleva et al., 2009b; Garsia et al., 2012; Tomasi et al., 2015). The processes of soot sedimentation on the ground and appearance of blanked patches from burning produce changes in the surface reflectance and possible variations in the radiative characteristics of the atmosphere. A detailed discussion of these problems is beyond the scope of the present work; therefore, all calculations below were performed for the same surface albedos $A_{s,\lambda}$, specified using multiyear data of MODIS satellite measurements for the region of Tomsk in June – August (Moody et al., 2005).

Data of Fontenla et al. (1999) were used to account for the spectral behavior of the solar constant.

The applicability of the algorithm and the approach to specifying the set of input parameters was confirmed by our earlier results of the complex radiation experiments (Zhuravleva et al., 2009a, 2014).

5.2 Simulation results

Recent studies showed that consideration of only specific spectral range of aerosol properties and neglect of uncertainties in specifying the input parameters (aerosol optical characteristics, surface albedo, total content and vertical profiles of concentrations of atmospheric gases, etc.) may be important error sources in estimates of aerosol radiation effects (Myhre et al., 2003; Zhou et al., 2005; Garcia et al., 2008, 2012; Zhuravleva et al., 2009ab). Magnitude of these errors depends mainly on aerosol type (background continental, oceanic, biomass burning, urban-industrial, desert dust, etc.), reflection model, and albedo of underlying surface, as well as on solar zenith angle (see, e.g., Garsia et al., 2008, 2012, 2014; Zhuravleva and Sakerin, 2009b).

In this work, we present the *diurnally* average radiative effects for 5 different situations (Table 4). To estimate correctly their uncertainties, it is necessary to take into account both variations in the characteristics of the atmosphere and underlying surface during the day and the dependence of uncertainties on the solar zenith angle. The estimates, presented in the literature, were generally obtained for fixed illumination conditions (see, e.g., Garsia et al., 2008, 2012, 2014; Zhuravleva and Sakerin, 2009b), while uncertainty estimates for *diurnally* average radiative effects are scarce (see, e.g., Tomasi et al., 2015, Esteve et., al., 2016). In this work, we restrict ourselves to a discussion of just radiation effects in different situations. Issue of what is the magnitude of uncertainty due to inaccurate information on input parameters of the problem needs additional numerical experiments and is beyond the scope of the present work.

Average values of AOD, W, SSA, and AF, which reflect the “average” radiative effects of smoke and background aerosol, were chosen as input parameters for the first three cases. In order to avoid the effect of astronomical factor, the instantaneous values of $F_{TOA(BOA)}^{\downarrow(\uparrow)}$ were calculated for period between sunrise and

Atmos. Meas. Tech. Discuss., doi:10.5194/amt-2016-244, 2016
Manuscript under review for journal Atmos. Meas. Tech.
Published: 15 August 2016

Atmospheric Measurement Techniques Discussions

sunset on July 15 for the latitude of Tomsk (56° N). Cases 4 and 5 correspond to the conditions of strong (July, 27) and relatively weak (July, 14) aerosol turbidity and, as such, make it possible to estimate the variability range of radiative characteristics in the period of smoke mist.

Figure 12 shows how radiation characteristics of the atmosphere and underlying surface are redistributed under different conditions.

The atmospheric transmittance (and, hence, ABS_{SUR}) was maximal (71%) under the background conditions. The appearance of optically dense smoke cloud had a consequence that *T* decreased to 60% (Case 3). Immediately in the period of 2012 smoke mist, the *T* value varied from 67% (July 14) to 37% (July 27), being almost a factor of two smaller in the latter case than under the background conditions. Data of calculations agree with results of measurements of total radiative fluxes in Tomsk (Sklyadneva et al., 2015), which indicated that on July 27, 2012 the total radiation decreased by about 50% relative to the usual conditions. Atmospheric albedo was also maximal (34%) on this day.

In analysis of ABS_{ATM}, the existence of two competing factors should be taken into consideration. If we represent the atmospheric absorption as a series in the order of scattering, its *n*th term will be proportional to $\omega_\lambda^{n-1}(1-\omega_\lambda)$; and for large ω_λ the contribution of high orders of scattering will be significant. Therefore, AOD increase (and, consequently, increment in the average order of scattering) favors absorption growth due to the contribution of high orders of scattering. At the same time, large SSA values act as a factor reducing the atmospheric absorptance.

The ABS_{ATM} value, calculated with averaged parameters, increased from 22% (Case 1) to 26% (Case 3); while for certain situations during summer 2012 the atmospheric absorptance varied in the range of 24-36%. A substantial increment in ABS_{ATM} on July 27 had been a consequence of a considerable (almost an order of magnitude) increase in AOD, accompanied by growth of the average order of scattering.

The direct radiative effect of aerosol for fixed characteristics of underlying surface and fixed solar zenith angle primarily depends on AOD, single scattering albedo, and asymmetry factor (Zhou et al., 2005; Yu et al., 2006; Tomasi et al., 2015). The results, presented in Fig. 12b, show a cooling effect of aerosol at the top and bottom of the atmosphere. As expected, the interrelation between DRE values was determined by aerosol optical depth and had been maximal (in absolute value) on July 27, 2012: $\Phi_{BOA} = -150$ W m^{-2}, $\Phi_{TOA} = -75$ W m^{-2}, $\Phi_{ATM} = 75$ W m^{-2}. Under the background conditions, the DRE value was minimal: -13 W m^{-2} at BOA and -5 W m^{-2} at TOA.

The AOD influence on direct radiative effect efficiency Φ^e, as compared to DRE, is much less pronounced, making it possible to estimate the influence of absorbing and scattering aerosol properties on radiative effects. However, it should be kept in mind that the increase of multiple scattering effects and attenuation of the transmitted radiation for large AOD moderate their effect (Conant et al., 2003).

For small atmospheric turbidity, the aerosol single scattering albedo weakly influences the radiative effect efficiency, and high $|\Phi^e|$ values at TOA, BOA, and in the atmosphere are primarily determined by AOD

Atmos. Meas. Tech. Discuss., doi:10.5194/amt-2016-244, 2016
Manuscript under review for journal Atmos. Meas. Tech.
Published: 15 August 2016

Atmospheric Measurement Techniques Discussions

(Case 1, Fig. 12c). The increase of efficiency for lowest AOD range was also noted by other authors (see, e.g., Garcia et al., 2012; background continental regions).

The aerosol optical depths in the ordinary smokes and on July 14 are close in value, whereas SSA values substantially differ (Table 4). A consequence of this is the inequality $\left|\Phi^e(\text{Case}\,2)\right| > \left|\Phi^e(\text{Case}\,4)\right|$, primarily because of higher absorptance of aerosol particles in ordinary smokes. Comparison of cases 3-5 shows that the $\left|\Phi^e(\text{Case}\,4)\right|$ value is maximal for SSA close to unity (Fig. 12c), suggesting that the influence of absorbing and scattering aerosol properties on radiative effect efficiency is moderated for high AOD values.

6 Conclusion

Previous studies showed that smokes from vegetation burning, together with large volcanic eruptions, are most intense natural sources of aerosol-gas emissions in boreal zones of the planet; they strongly influence the radiation budget on the scales of large regions a few weeks long. One such event, i.e., smoke mist due to massive forest fires, had taken place during summer 2012 in a few Siberian regions.

In this work, we present the results of complex study of the optical and microphysical characteristics and radiation effects of aerosol, observed under the conditions of severe smoke turbidity of the atmosphere. The basis for analysis had been photometric observations (AERONET/Tomsk-22) of spectral solar radiation with the use of the algorithms of solution of inverse problems of atmospheric optics and model calculations of the main components of shortwave radiation budget. The obtained radiation characteristics in smoke mist situation are compared with data of multiyear (2003-2013) observations under the background conditions, for “ordinary” smokes, as well as with results of studying the smoke aerosol obtained by other authors.

Intensive wildfires in 2012 in Siberia had led to extremely high aerosol loading of the atmosphere: the average AOD(500 nm) in the period of smoke mist had been 0.95±0.86, a factor of 6 larger than under the background conditions (0.16±0.08), and almost a factor of 2.5 larger than AOD in “ordinary” smokes (0.36±0.18). The AOD value exceeded 3 in certain periods of measurements (on July 24-28).

Like at other AERONET sites, where smoke aerosol was recorded, in Tomsk the volume aerosol size distributions were bimodal with dominating fine-mode fraction. In June-August 2012, the mean median radius of fine fraction r_v^f had increased to 0.18 μm as compared to “ordinary” smokes ($r_v^f = 0.16\ \mu m$). The width of the fine mode distribution increased, as was the case in period of intense fires during summer 2004-2005 in Alaska [Eck et al., 2009]. In contrast to data of multiyear observations, in summer 2012 an increase in the volume concentration and median radius of the coarse mode was observed with the growing AOD.

The average imaginary refractive index of the Tomsk smoke mist shows low values and relatively large decrease in κ_λ as the wavelength grows from 440 nm (0.0067) to 675 nm (0.0054). The κ_λ variations in the wavelength interval of 675-1020 m are not as strong. At the same time, in ordinary smokes the imaginary part of refractive index showed spectral behavior close to neutral one ($\kappa_\lambda \approx 0.01$).

A consequence of small values of the imaginary index of refraction coupled with the large fine-mode

Atmos. Meas. Tech. Discuss., doi:10.5194/amt-2016-244, 2016
Manuscript under review for journal Atmos. Meas. Tech.
Published: 15 August 2016

Atmospheric Measurement Techniques Discussions

particle radius had been, on the average, quite high single scattering albedos of smoke aerosol, weakly varying with wavelength (0.96). A similar situation was also observed at other AERONET sites, located in boreal zone of Eurasia, during extended wildfires: Moscow (2002 and 2010), Alaska (2004 and 2005). At the same time, increasing spectral behavior of single scattering albedo with the growing wavelength was observed in certain periods of smoke turbidities. Possibly, this spectral dependence was because "brown" carbon, which absorbs most intensely in ultraviolet spectral region, was present in the atmosphere. A comparative analysis also showed that SSA values and their spectral dependence differ between smoke mist and "ordinary" smokes. In the latter case, the increase in absorptance of aerosol particles and decrease in SSA with the growing wavelength well correspond to the character of SSA variations, recorded in boreal zone of USA and Canada according to data of multiyear observations (Dubovik et al., 2002).

Such extraordinary events as severe smoke mist (Siberia, 2012; Moscow, 2010; etc.) are quite rare in occurrence. However, when optical and microphysical characteristics, obtained in these periods of time, are included in the total dataset (ordinary smokes, usual conditions), this may introduce substantial changes in the statistical characteristics of aerosol, typical for a given region (see, e.g., Sayer et al., 2014), and will lead to a greater uncertainty in estimates of radiation-climatic effects of aerosol. In our opinion, it is more correct to use the obtained information for analysis of characteristics of "pure" smoke aerosol (in view of its predominating contribution), as well as for estimation of maximal radiation effect of smokes.

The results of simulating the diurnally average radiative characteristics, presented in the work, reflect the "average" radiative effects of smoke and background aerosol. As compared to background conditions and "ordinary" smokes, under the conditions of smoke mist the cooling effect of aerosol intensifies (predominately due to a substantial increase in AOD): direct radiative effects at the bottom and top of the atmosphere are -13, -35, and - 60 W m^{-2}, and -5, -14, and -35 W m^{-2} respectively. Values of direct radiative effect efficiency Φ^e under the background conditions and under the conditions of ordinary smokes are comparable (Φ^e_{BOA} ~-100 W m^{-2}, Φ^e_{TOA} ~-40 W m^{-2}, Φ^e_{ATM} ~-60 W m^{-2}), while in smoke mist the increase in single scattering albedo leads to almost halving of Φ^e_{ATM}. We note that this work presents estimates of daytime values of aerosol radiation effects under different atmospheric situations. The issue of what is the uncertainty of these estimates, caused by insufficiently exact information on the input parameters of radiation calculations, requires further study.

References

Anderson, G., Clough, S., Kneizys, F., Chetwynd, J., and Shettle, E.: AFGL Atmospheric Constituent Profiles (0 - 120 km), Air Force Geophysics Laboratory, AFGL-TR-86-0110, Environmental Research Paper, N 954, 1986.

Andreae, M. O. and Gelencsér, A.: Black carbon or brown carbon? The nature of light-absorbing carbonaceous aerosols, Atmos. Chem. Phys., 6, 3131–3148, doi:10.5194/acp-6-3131-2006, 2006.

Atmos. Meas. Tech. Discuss., doi:10.5194/amt-2016-244, 2016
Manuscript under review for journal Atmos. Meas. Tech.
Published: 15 August 2016

Atmospheric Measurement Techniques Discussions

641 Arshinov, M. Yu., Belan, B. D., Davydov, D. K., Inouye, G., Maksyutov Sh., Machida T., and Fofonov A. V.:
642 Vertical distribution of greenhouse gases above Western Siberia by the long-term measurement data,
643 Atmos. Ocean. Opt., 22, 316–324, 2009.

644 Bedareva, T.V, Sviridenkov, M.A, and Zhuravleva, T.B.: Retrieval of aerosol optical and microphysical
645 characteristics according to data of ground-based spectral measurements of direct and scattered solar
646 radiation. Part 1. Testing of Algorithm, Atmos. Ocean. Opt., 26, 24-34, 2013a.

647 Bedareva, T.V, Sviridenkov, M.A., and Zhuravleva, T.B.: Retrieval of aerosol optical and microphysical
648 characteristics according to data of ground-based spectral measurements of direct and scattered solar
649 radiation. Part 2. Approbation of Algorithm, Atmos. Ocean. Opt., 26, 107-117, 2013b.

650 Bedareva, T.V., Sviridenkov, M.A., Zhuravleva, T.B.: Retrieval of dust aerosol optical and microphysical
651 properties from ground-based Sun-sky radiometer measurements in approximation of randomly oriented
652 spheroids, J. Quantitative Spectroscopy and Radiative Transfer, 146, 140-157, doi:
653 10.1016/j.jqsrt.2014.05.006, 2014.

654 Bergstrom, R. W., Russell, P. B., and Hignett, P.: Wavelength dependence of the absorption of black carbon
655 particles: Predictions and results from the TARFOX experiment and implications for the aerosol single
656 scattering albedo, J. Atmos. Sci., 59, 567–577, 2002.

657 Bergstrom, R. W., Pilewskie, P., Russell, P. B., Redemann, J., Bond, T. C., Quinn, P. K., and Sierau, B.:
658 Spectral absorption properties of atmospheric aerosols, Atmos. Chem. Phys., 7,5937–5943,
659 doi:10.5194/acp-7-5937-2007, 2007.

660 Bond, T. C.: Spectral dependence of visible light absorption by carbonaceous particles emitted from coal
661 combustion, Geophys. Res. Lett., 28, 4075–4078, 2001.

662 Bond, T. C. and Bergstrom, R. W.: Light Absorption by Carbonaceous Particles: An Investigative Review,
663 Aerosol Science and Technology, 40(1), 27–67, doi: 10.1080/02786820500421521, 2006.

664 Chen, Y. and Bond, T. C.: Light absorption by organic carbon from wood combustion, Atmos. Chem. Phys.,
665 10, 1773–1787, doi:10.5194/acp-10-1773-2010, 2010.

666 Chubarova, N., Smirnov, A., and Holben, B. N.: Aerosol properties in Moscow according to 10 years of
667 AERONET measurements at the meteorological observatory of Moscow state university, Geography,
668 Enviroment, Sustainability, 4 (1), 19–32, 2011.

669 Chubarova, N., Nezval', E., Sviridenkov, M., Smirnov, A., and Slutsker, I: Smoke Aerosol and its Radiative
670 Effects During Extreme Fire Event over Central Russia in Summer 2010, Atmos. Meas. Tech., 5, 557–568,
671 doi:10.5194/amt-5-557-2012, 2012.

672 Conant, W. C., Seinfeld, J. H., Wang, J. , Carmichael, G. R., Tang, Y. , Uno, I., Flatau, P. J., Markowicz, K.
673 M., and Quinn, P. K.: A model for the radiative forcing during ACE-Asia derived from CIRPAS Twin
674 Otter and R/V Ronald H. Brown data and comparison with observations, J. Geophys. Res., *108*(D23),
675 8661, doi:10.1029/2002JD003260, 2003.

676 Dubovik, O.T. and King, M.: A flexible inversion algorithm for retrieval aerosol optical properties from Sun
677 and sky radiance measurements, J. Geophys. Res., 105 (D16), 20673-20696, 2000.

678 Dubovik, O., Smirnov, A., Holben, B., King, M., Kaufman, Y., Eck, T., and Slutsker, I.: Accuracy assessments
679 of aerosol optical properties retrieved from Aerosol Robostic Network (AERONET) Sun and sky radiance
680 measurements, J. Geophys. Res., 105 (D8), 9791-9806, 2000a.

681 Dubovik, O., Holben, B., Eck, T., Smirnov, A., Kaufman, Y., King, M., Tanré, D., and Slutsker I.: Variability
682 of absorption and optical properties of key aerosol types observed in worldwide locations, J. Atmos. Sci.,
683 59 (3), 590-608, 2002.

684 Eck, T. F., Holben, B. N., Reid, J. S., Sinyuk, A., Hyer, E. J., O'Neill, N. T., Shaw, G. E., Vande Castle, J.
685 R., Chapin, F. S., Dubovik, O., Smirnov, A., Vermote, E., Schafer, J. S., Giles, D., Slutsker, I.,
686 Sorokine, M., and Newcomb, W. W.: Optical properties of boreal region biomass burning aerosols in
687 central Alaska and seasonal variation of aerosol optical depth at an Arctic coastal site, J. Geophys. Res.,
688 114, D11201, doi:10.1029/2008JD010870, 2009.

689 Esteve, A.R., Highwood, E.J., and Ryder, C.L.: A case study of the radiative effect of aerosols over Europe:
690 EUCAARI-LONGREX, Atmos. Chem. Phys., 16, 7639–7651, 2016.

691 Fontenla, J., White, O.R., Fox, P.A., Avert, E.H., and Kurucz, R.L.: Calculation of solar irradiances, I.
692 Synthesis of the solar spectrum, Astrophys. J., 518, 480-500, 1999.

693 Garcıa, O. E., Dıaz, A. M., Exposito, F. J., Dıaz, J. P., Dubovik, O., Dubuisson, P., Roger, J.-C., Eck, T. F.,
694 Sinyuk, A., Derimian, Y., Dutton, E. G., Schafer, J. S., Holben, B. N., and Garcıa, C. A.: Validation of
695 AERONET estimates of atmospheric solar fluxes and aerosol radiative forcing by ground-based broadband
696 measurements, J. Geophys. Res., 113, D21207, doi:10.1029/2008JD010211, 2008.

697 Garcıa, O. E., Dıaz, A. M., Exposito, F. J., Dubovik, O., Derimian, Y., Dubuisson, P., and Roger, J.-C.:
698 Shortwave radiative forcing and efficiency of key aerosol types using AERONET data, Atmos. Chem.
699 Phys., 12, 5129–5145, doi:10.5194/acp-12-5129-2012, 2012.

700 Garcia, R. D., Garcia, O. E., Cuevas, E., Cachorro, V. E., Romero-Campos, P. M., Ramos, R. and de Frutos,
701 A. M.: Solar radiation measurements compared to simulations at the BSRN Izana station: Mineral dust
702 radiative forcing and efficiency study, J. Geophys. Res., 119, 179–194, doi:10.1002/2013JD020301, 2014

703 Giles, D. M., Holben, B. N., Eck, T. F., Sinyuk, A., Smirnov, A., Slutsker, I., Dickerson, R. R., Thompson,
704 A. M., and Schafer, J. S.: An analysis of AERONET aerosol absorption properties and classifications
705 representative of aerosol source regions, J. Geophys. Res., 117, D17203, doi:10.1029/2012JD018127,
706 2012.

707 Gorchakov, G.I., Sitnov, S.A., Sviridenkov, M.A., Semoutnikova, E.G., Emilenko, A.S., Isakov, A.A.,
708 Kopeikin, V.M., Karpov, A.V., Gorchakova, I.A., Verichev, K.S., Kurbatov, G.A., and Ponomareva,
709 T.Ya.: Satellite and ground-based monitoring of smoke in the atmosphere during the summer wildfires in
710 European Russia in 2010 and Siberia in 2012, Int. J. Remote Sensing, 35(15), 5698-5721, 2014.

711 Groisman, P. Ya., Sherstyukov, B. G., Razuvaev, V. N., Knight, R.W., Enloe, J.G., Stroumentova, N.S.,
712 Whitfield, P.H., Førland, E., Hannsen –Bauer, I., Tuomenvirt, H., Aleksandersson, H., Mescherskaya, A.,
713 and Karl, T.R.: Potential forest fire danger over Northern Eurasia: Changes during the 20th century, Global
714 and Planet. Change, 56, 371–386, 2007.

715 Hammer, M. S., Martin, R. V., van Donkelaar, A., Buchard, V., Torres, O., Ridley, D. A., and Spurr, R. J. D.:
716 Interpreting the Ultraviolet Aerosol Index observed with the OMI satellite instrument to understand
717 absorption by organic aerosols: implications for atmospheric oxidation and direct radiative effects, Atmos.
718 Chem. Phys., 16, 2507–2523, doi:10.5194/acp-16-2507-2016, 2016.

719 Hess, M., Koepke, P., and Schult, I.: Optical properties of aerosols and clouds: The software package OPAC,
720 Bull. Amer. Meteorol. Soc., 79, 831-844, 1998.

721 Holben, B.N., Eck, T.F., Slutsker, I., Tanre, D., Buis, J.P., Setzer, A., Vermote, E., Reagan, J.A., Kaufman,
722 Y.J., Nakadjima, T., Lavenu, F., Jankowiak, I., and Smirnov, A.: AERONET - A federated instrument
723 network and data archive for aerosol characterization, Rem. Sens. Env., 66(1), 1-16, 1998.

724 Holben, B. N., Eck, T. F., Slutsker, I., Smirnov, A., Sinyuk, A., Schafer, J., Giles, D., and Dubovik, O.:
725 AERONET's Version 2.0 quality assurance criteria, Remote Sensing of Atmosphere and Clouds, edited by
726 S.-C. Tsay et al., Proc. SPIE, 6408, 64080Q, doi:10.1117/12.706524, 2006.

727 Jethva, H. and Torres, O.: Satellite-based evidence of wavelength-dependent aerosol absorptionin biomass
728 burning smoke inferred from Ozone Monitoring Instrument, Atmos. Chem. Phys., 11, 10541–10551,
729 doi:10.5194/acp-11-10541-2011, 2011.

730 Kabanov, D.M. and Sakerin, S.M.: Variations of the characteristics of the aerosol optical depth under
731 conditions of forest fires, Proc. of SPIE: Thirteenth Joint International Symposium on Atmospheric and
732 Ocean Optics. Atmospheric Physics, 6522, 65221J-1 – 65221J-6, 2006.

733 Kirchstetter, T. W., Novakov, T., and Hobbs, P. V.: Evidence that the spectral dependence of light absorption
734 by aerosols is affected by organic carbon, J. Geophys. Res., 109, D21208, doi: 10.1029/ 2004jd004999,
735 2004.

736 Komarov, V.S. and Lomakina, N.Ya.: Statistical models of the atmospheric boundary layer, IAO Publishing
737 House, Tomsk, 2008 (in Russian).

738 Kozlov, V.S., Yausheva, E. P., Terpugova, S.A., Panchenko, M.V., Chernov, D.G., and Shmargunov V.P.:
739 Optical–microphysical properties of smoke haze from Siberian forest fires in summer 2012, Int. J. Remote
740 Sensing, 35(15), 5722-5741, 2014.

741 Lewis, K., Arnott, W. P., Moosmuller, H., and Wold, C. E.: Strong spectral variation of biomass smoke light
742 absorption and single scattering albedo observed with a novel dual-wavelength photoacoustic instrument, J.
743 Geophys. Res., 113, D16203 doi: 10.1029/ 2007jd009699, 2008.

744 Lu,Z., Streets, D.J., Winijkul E., Yan, F., Chen, Y., Bond, T.C., Feng, Y., Dubey, M.K., Liu, S., Pinto, J.P.,
745 and Carmichael G.R.: Light Absorption Properties and Radiative Effects of Primary Organic Aerosol
746 Emissions, Environ. Sci. Technol., 49, 4868−4877 DOI: 10.1021/acs.est.5b00211, 2015.

747 Myhre, G., Berntsen, T. K., Haywood, J. M., Sundet, J. K., Holben, B. N., Johnsrud, M., and Stordal, F.:
748 Modeling the solar radiative impact of aerosols from biomass burning during the Southern African
749 Regional Science Initiative (SAFARI-2000) experiment, J. Geophys. Res., 108(D13), 8501,
750 doi:10.1029/2002JD002313, 2003.

751 Moody, E.G., King, M.D., Platnick, S., Schaaf, C.B., and Gao F.: Spatially compete global spectral surface
752 albedos: value-added datasets derived from Terra MODIS Land products, IEEE T. Geosci. Remote Sens.,
753 43, 144-158, 2005.

754 Moosmu¨ller, H, Chakrabarty, R.K., and Arnott, W.P.: Aerosol light absorption and its measurement: A
755 review, Journal of Quantitative Spectroscopy and Radiative Transfer, 110, 844–878, 2009.

756 Nikonovas, T., North, P. R. J., and Doerr, S. H.: Smoke aerosol properties and ageing effects for northern
757 temperate and boreal regions derived from AERONET source and age attribution, Atmos. Chem. Phys., 15,
758 7929–7943, doi:10.5194/acp-15-7929-2015, 2015.

759 O'Neill, N. T., Eck, T. F., Holben, B. N., Smirnov, A., Dubovik, O., and Royer, A.: Bimodal size
760 distribution influences on the variation of Angstrom derivatives in spectral and optical depth space, J.
761 Geophys. Res., 106, 9787–9806, doi:10.1029/2000JD900245, 2001.

762 O'Neill, N. T., Eck, T. F., Smirnov, A., Holben, B. N., and Thulasiraman, S.: Spectral discrimination of
763 coarse and fine mode optical depth, J. Geophys. Res., 108(D17), 4559, doi:10.1029/2002JD002975, 2003.

764 Panchenko, M. V., Zhuravleva, T. B., Terpugova, S. A., Polkin, V. V., and Kozlov, V. S.: An empirical model
765 of optical and radiative characteristics of the tropospheric aerosol over West Siberia in summer, Atmos.
766 Meas. Tech., 5, 1513-1527, doi:10.5194/amt-5-1513-2012, 2012.

767 Panchenko M. V., Zhuravleva, T. B., Kozlov, V. S. , Nasrtdinov, I. M., Pol'kin, V. V., Terpugova, S. A., and
768 Chernov, D. G.: Estimation of Aerosol Radiation Effects under Background and Smoke-haze Atmospheric
769 Conditions over Siberia from Empirical Data, Russian Meteorology and Hydrology, 41 (2), 104–111, 2016.

770 Polyakov, D. V., Barashkova, N. K., and Kuzhevskaya, I. V.: Weather and Climate Description of Anomalous
771 Summer 2012 in Tomsk Region, Russian Meteorology and Hydrology, 39(1), 22–28, 2014.

772 Reid, J. S., Hobbs, P. V., Ferek, R. J., Blake, D. R., Martins, J. V., Dunlap, M. R., and Liousse, C.: Physical,
773 chemical, and optical properties of regional hazes dominated by smoke in Brazil, J. Geophys. Res., 103,
774 32059–32080, 1998.

775 Reid, J. S., Koppmann, R., Eck, T. F., and Eleuterio, D. P.: A review of biomass burning emissions: Part II.
776 Intensive physical properties of biomass burning particles, Atmos. Chem. Phys., 5, 799–825, 2005.

777 Reid, J. S., Eck, T. F., Christopher, S. A., Koppmann, R., Dubovik, O., Eleuterio, D. P., Holben, B. N., Reid,
778 E. A., and Zhang, J.: A review of biomass burning emissions: Part III. Intensive optical properties of
779 biomass burning particles, Atmos. Chem. Phys., 5, 827–849. 2005a.

780 Rothman, L.S., Gordon, I.E., Babikov, Y., Barbe, A., Benner, D. C., Bernath, P.F., Birk M. et.al.: The
781 HITRAN 2012 molecular spectroscopic data base, Journal of Quantitative Spectroscopy and Radiative
782 Transfer,130, 4–50, 2013.

783 Russell, P. B., Bergstrom, R. W., Shinozuka, Y., Clarke, A. D., De-Carlo, P. F., Jimenez, J. L., Livingston, J.
784 M., Redemann, J., Dubovik, O., and Strawa, A.: Absorption Angstrom Exponent in AERONET and related
785 data as an indicator of aerosol composition, Atmos. Chem. Phys., 10, 1155–1169, doi:10.5194/acp-10-
786 1155-2010, 2010.

787 Sakerin, S.M. and Kabanov D.M.: Spectral dependence of the atmosphere aerosol optical depth near 0.37–4
788 μm, Atmos. Ocean. Opt., 20, 141-149, 2007.

789 Sakerin, S.M., Beresnev, S.A., Gorda, S.Yu., Kabanov, D.M., Kornienko, G.I., Markelov, Yu.I., Mikhalev,
790 A.V., Nikolashkin, S.V., Panchenko, M.V., Poddubnyi, V.A., Pol'kin, V.V., Smirnov, A., Tashchilin,
791 M.A., Turchinovich, S.A., Turchinovich, Yu. S., Holben, B., and Eremina, T.A.: Characteristics of the
792 annual behavior of the spectral aerosol optical depth of the atmosphere under conditions of Siberia,
793 Atmos. Ocean. Opt., 22(4), 446–456, 2009.

794 Sakerin, S.M., Kabanov, D.M., Nasrtdinov, I.M., Turchinovich, S.A., and Turchinovich, Yu. S.: The results of
795 two-point experiments on the estimation of the urban anthropogenic effect on the characteristics of
796 atmospheric transparency, Atmos. and Ocean. Opt., 23(2), 88-94, 2010.

797 Sakerin., S.M. (Ed.): Study of radiative characteristics of aerosol in Asian part of Russia, Publishing House of
798 Institute of Atmospheric Optics SB RAS, 484, 2012 (in Russian).

799 Sakerin, S.M., Andreev, S.Yu., Kabanov, D.M., Nikolashkin, S.V., Prakhov, A.N., Radionov, V.F.,
800 Turchinovich, Yu.S., Chernov, D.G., Holben, B.N., and Smirnov, A.: On results of studies of
801 atmospheric aerosol optical depth in arctic regions, Atmos. Ocean. Opt., 27(6), 517-528, 2014.

802 Sakerin, S.M., and Kabanov, D.M. Finely and coarsely dispersed components of atmospheric aerosol optical
803 depth in the region of Tomsk: interannual and seasonal variations, Proc. of SPIE, 9680, doi:
804 10.1117/12.22050, 2015.

805 Sayer, A. M., Hsu, N. C., Eck, T. F., Smirnov, A., and Holben, B. N.: AERONET-based models of smoke-
806 dominated aerosol near source regions and transported over oceans, and implications for satellite retrievals
807 of aerosol optical depth, Atmos. Chem. Phys., 14, 11493–11523, doi:10.5194/acp-14-11493-2014, 2014.

808 Schuster, G. L., Dubovik, O., and Arola, A.: Remote sensing of soot carbon. Part 1: Distinguishing different
809 absorbing aerosol species, Atmos. Chem. Phys., 16, 1565–1585, 2016

810 Shakina, N. P. and A. R. Ivanova: The Blocking Anticyclones: the State of Studies and Forecasting, Russian
811 Meteorology and Hydrology, 35(11), 721–730, 2010.

812 Sklyadneva, T.K., Ivlev, G.A., Belan, B.D., Arshinov, M.Yu., and Simonenkov, D.V.: The radiation regime of
813 Tomsk in conditions of a smoky haze, Atmos. Ocean. Opt., 28(03), 215-222, 2015 (in Russian)/

814 Smirnov, A., Holben, B. N., Eck, T. F., Dubovik, O., and Slutsker, I.: Cloud screening and quality control
815 algorithms for the AERONET data base, Remote Sens. Environ., 73, 337–349, 2000.

816 Tomasi, C., Lanconelli, C., Lupi, A., and Mazzola, M.: Diurnally averaged direct aerosol-induced radiative
817 forcing from cloud-free sky field measurements performed during seven regional experiments, in: Light
818 Scattering Reviews 9, Ed. Kokhanovsky, A. Springer Praxis Books, 297-425, 2015.

819 Torres, O., Bhartia, P. K., Herman, J. R., Ahmad, Z., and Gleason, J.: Derivation of aerosol propertiesfrom
820 satellite measurements of backscattered ultraviolet radiation: theoretical basis, J. Geophys. Res., 103,
821 doi:10.1029/98JD00900, 1998.

822 Tvorogov, S.D., Zhuravleva, T.B., Rodimova, O.B., and Firsov, K.M.: Theory of series of exponents and its
823 application for analysis of radiation processes, in: Problems of Global Climatology and Ecodynamics.
824 Anthropogenic Effects on the State of Planet Earth, A.P. Cracknell, V.F. Krapivin, and C.A. Varotsos
825 (eds), Springer/Praxis, Chichester, UK, 211-240, 2008.

826 Vinogradova, A. A., Smirnov, N. S., Korotkov, V. N., and A. A. Romanovskaya: Forest Fires in Siberia and
827 the Far East: Emissions and Atmospheric Transport of Black Carbon to the Arctic, Atmos. Ocean. Opt., 28
828 (6), 566–574, 2015.

829 Yu, H., Kaufman, Y., Chin, M., Feingold, G., Remer, L., Anderson, T., Balkanski, Y., Bellouin, N., Boucher,
830 O., Christopher, S., DeCola, P., Kahn, R., Koch, D., Loeb, N., Reddy, M., Schulz, M., Takemura, T., and
831 Zhou, M. A review of measurement-based assessments of the aerosol direct radiative effect and forcing,
832 Atmos. Chem. Phys., 6, 613-666, 2006.

833 Zhong, M. and Jang, M.: Dynamic light absorption of biomass-burning organic carbon photochemically aged
834 under natural sunlight, Atmos. Chem. Phys., 14, 1517–1525, doi:10.5194/acp-14-1517-2014, 2014.

Atmos. Meas. Tech. Discuss., doi:10.5194/amt-2016-244, 2016
Manuscript under review for journal Atmos. Meas. Tech.
Published: 15 August 2016

Atmospheric Measurement Techniques Discussions

835 Zhou M., Yu H., Dickinson, R., Dubovik, O., Holben, B.: A normalized description of the direct effect of key
836 aerosol types on solar radiation as estimated from AERONET aerosols and MODIS albedo, J. Geophys.
837 Res., 110, doi:10.1029/2005JD005909, 2005.

838 Zhuravleva, T.B., Kabanov, D.M., Sakerin, S.M., and Firsov, K.M.: Simulation of direct aerosol radiative
839 forcing for typical summer conditions of Siberia. Part 1: Method of calculation and choice of the input
840 parameters, Atmos. .Ocean. Opt., 22, 63-73, 2009a.

841 Zhuravleva, T.B. and Sakerin, S.M..: Simulation of direct aerosol radiative forcing for typical summer
842 conditions of Siberia. Part II: Variability range and sensitivity to the input parameters, Atmos. Ocean. Opt,
843 22, 22(1), 74-83, 2009b.

844 Zhuravleva, T.B., Sakerin, S. M., Bedareva, T. V., Kabanov, D. M., Nasrtdinov, I.M., and Chesnokova, T. Yu.:
845 Solar radiative fluxes in the clear-sky atmosphere of Western Siberia: A comparison of simulations
846 with field measurements, Atmos. Ocean. Opt., 27(2), 176-186, 2014.

Atmos. Meas. Tech. Discuss., doi:10.5194/amt-2016-244, 2016
Manuscript under review for journal Atmos. Meas. Tech.
Published: 15 August 2016

Atmospheric Measurement Techniques Discussions

Table 1. Average (± SD) characteristics of AOD and water vapor content of the atmospherein the period of smoke mist in 2012 as compared to multiyear data for July and "ordinary" smokes (April-October 2003-2011 and 2013)

Characteristics	July, multiyear		Smoke mist (Jun 17 – Aug 6, 2012)	"Ordinary" smokes
	Background conditions	Total dataset (with smokes)		
τ_{340}	0.25±0.11	0.33±0.26	1.37±1.10	0.58±0.28
τ_{500}	0.16±0.08	0.21±0.18	0.95±0.86	0.36±0.18
τ_{870}	0.07±0.04	0.09±0.08	0.40±0.40	0.15±0.09
α	1.48±0.29	1.49±0.28	1.58±0.21	1.59±0.22
β	0.058±0.037	0.074±0.064	0.33±0.35	0.12±0.071
W, g/cm^2	2.09±0.56	2.16±0.57	2.19±0.58	1.93±0.79

Table 2. Average (±SD), minimal, and maximal values of AOD (550 nm) in different periods of 2012 smoke mist according to data of ground-based and satellite measurements over the central part of the Western Siberia

Period	Satellite data		Ground-based observations (Tomsk-22)	
	Average ± SD	min/max	Average ± SD	min/max
June 6-10	0.23±0.08	0.04/0.41	0.19 ± 0.07	0.10/0.27
July 1-4	1.40±0.62	0.18/3.25	1.51± 1.05	0.85/2.72
July 10-14	0.28±0.11	0.08/0.76	0.22± 0.11	0.11/0.35
July 24-28	1.19±1.08	0.00/3.63	2.74± 1.07	1.32/3.83

Atmos. Meas. Tech. Discuss., doi:10.5194/amt-2016-244, 2016
Manuscript under review for journal Atmos. Meas. Tech.
Published: 15 August 2016

Atmospheric Measurement Techniques Discussions

Table 3. Optical and microphysical properties of biomass burning aerosol retrieved from AERONET Tomsk sites ("Tomsk", "Tomsk-22")

Aerosol characteristics	Smoke mist, 2012	Ordinary smoke, 2003-2011,2013
n(440/675/870/1020)	1.469/1.486/1.503/1.499	1.454/1.471/1.485/1.499
κ(440/675/870/1020), ($\times 10^2$)	0.673/0.538/0.501/0.488	1.126/1.005/1.057/1.06
ω(440/675/870/1020)	0.96/0.96/0.95/0.95	0.92/0.91/0.89/0.88
g(440/675/870/1020)	0.68/0.59/0.54/0.51	0.68/0.59/0.55/0.54
$r_v^f\,(\mu\text{m})$, $\sigma^f\,(\mu\text{m})$	0.181±0.02; 0.507±0.058 $r_v^f = 0.166 + 0.017\tau_{440}$ (R=0.47)	0.161±0.030; 0.422±0.058 $r_v^f = 0.153 + 0.011\tau_{440}$ (R=0.13)
$r_v^c\,(\mu\text{m})$, $\sigma^c\,(\mu\text{m})$	3.321±0.365; 0.703±0.056 $r_v^c = 2.928 + 0.44\tau_{440}$ (R=0.66)	2.911±0.665; 0.694±0.077 $r_v^c = 3.10 - 0.249\tau_{440}$ (R=-0.13)
$C_v^f\left(\mu\text{m}^3/\mu\text{m}^2\right)$	0.11±0.065 $C_v^f = 0.009 + 0.114\tau_{440}$ (R=0.96)	0.097±0.042 $C_v^f = 0.017 + 0.106\tau_{440}$ (R=0.87)
$C_v^c\left(\mu\text{m}^3/\mu\text{m}^2\right)$	0.025±0.012 $C_v^c = 0.013 + 0.014\tau_{440}$ (R=0.62)	0.062±0.04 $C_v^c = 0.036 + 0.035\tau_{440}$ (R=0.24)

Table 4. Parameters of radiation calculations

	Case	τ_{550}	$\alpha_{440-870}$	W	ω_{550}	g_{550}
1	Background aerosol	0.13	1.46	2.1	0.925	0.7
2	"Ordinary" smokes	0.33	1.59	1.9	0.92	0.64
3	Smoke mist, 2012	0.84	1.58	2.2	0.96	0.64
4	July 14	0.34	1.74	2.5	0.98	0.64
5	July 27	3.54	1.54	1.2	0.94	0.65
Spectral surface albedo		$A_{s,470}$ =0.036; $A_{s,560}$ =0.067; $A_{s,670}$ =0.068; $A_{s,870}$ =0.251; $A_{s,1250}$ =0.285; $A_{s,1650}$ =0.196; $A_{s,2150}$ =0.1				

Atmos. Meas. Tech. Discuss., doi:10.5194/amt-2016-244, 2016
Manuscript under review for journal Atmos. Meas. Tech.
Published: 15 August 2016

Atmospheric Measurement Techniques Discussions

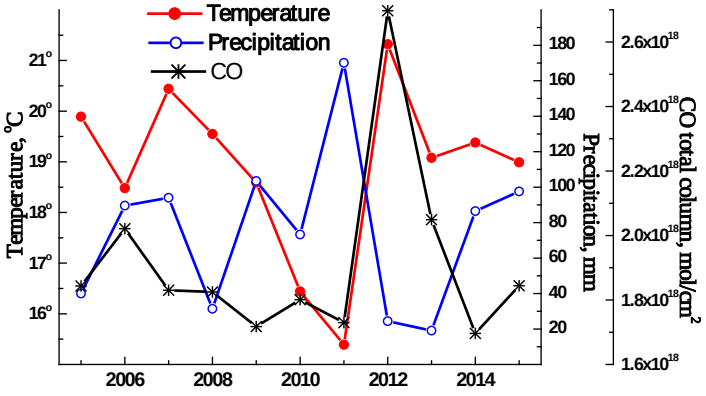

Figure 1. Interannual variations in July-average temperatures and precipitation amount according to data from "Tomsk" meteorological station, as well as interannual variations in total carbon monoxide content according to satellite observations over the territory of Tomsk region (http://giovanni.sci.gsfc.nasa.gov/).

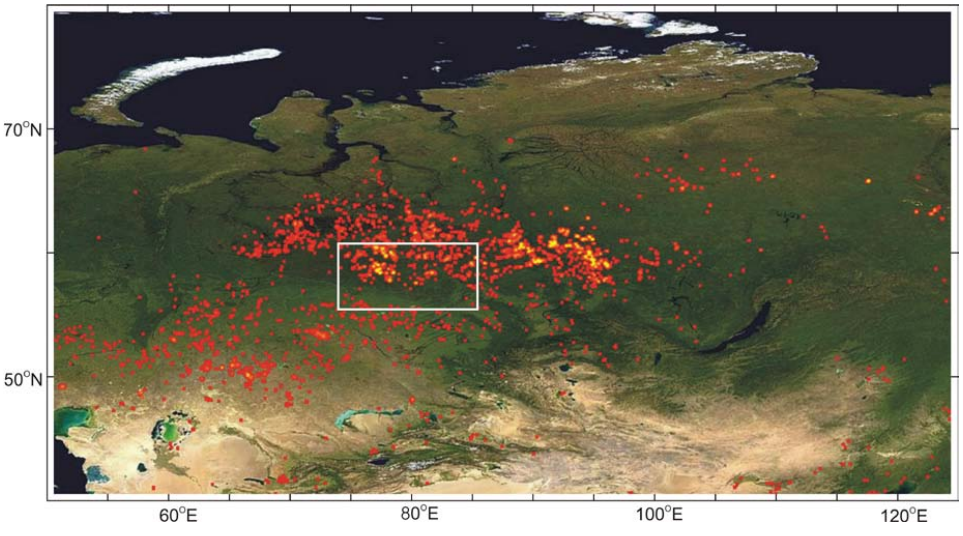

Figure 2. The map of forest fires over Siberia in the period from July 19 to 28, 2012 (http://lance-modis.eosdis.nasa.gov/cgi-bin/imagery/firemaps.cgi). The Tomsk region (56-61ºN; 75-88ºE) is highlighted by box.

Atmos. Meas. Tech. Discuss., doi:10.5194/amt-2016-244, 2016
Manuscript under review for journal Atmos. Meas. Tech.
Published: 15 August 2016

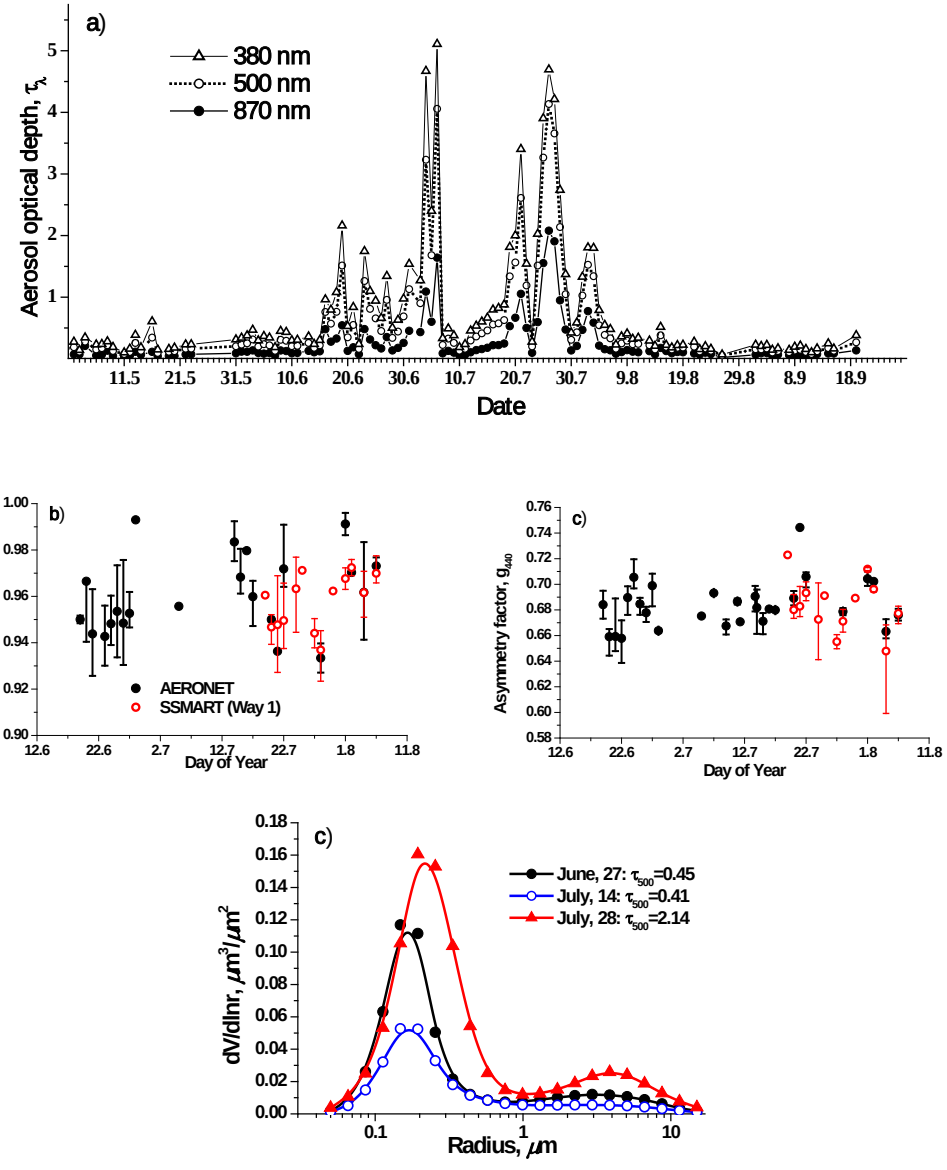

Figure 3. (a) Daily average AOD, (b) single scattering albedo and (c) asymmetry factor time series, and (d) examples of particle size distribution in "Tomsk-22" during summer period of 2012.

Atmos. Meas. Tech. Discuss., doi:10.5194/amt-2016-244, 2016
Manuscript under review for journal Atmos. Meas. Tech.
Published: 15 August 2016

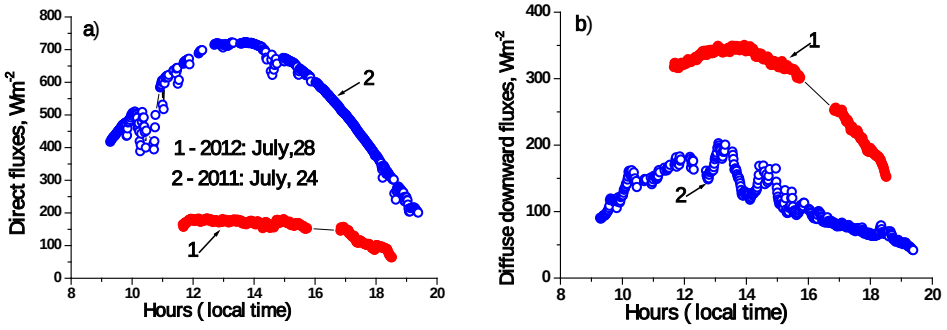

Figure 4. Daytime behavior of (a) direct and (b) diffuse fluxes of solar radiation under the usual conditions (July 24, 2011) and during smoke mist (July 28, 2012) in the region of "Fonovaya" observatory.

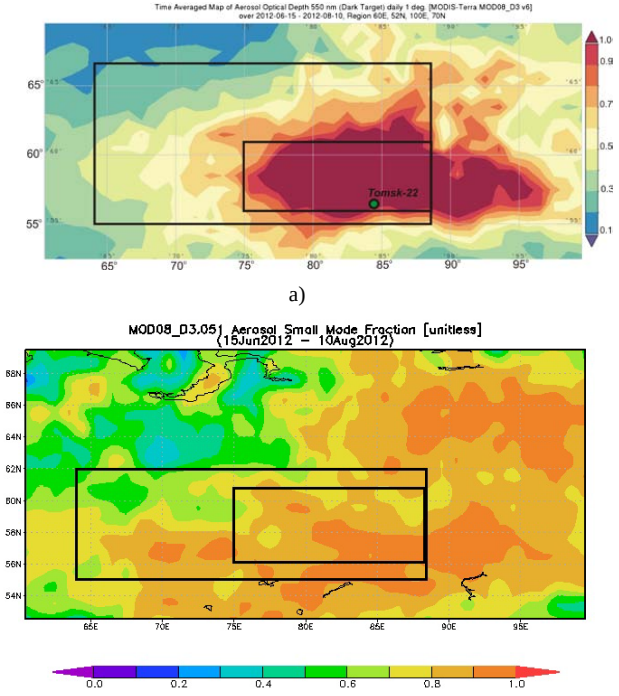

Figure 5. Spatial distributions of (a) AOD (MODIS collection 6) and (b) Aerosol Small Mode Fraction (MODIS collection 5) over Western and Eastern Siberia during June 15 – August 10, 2012. The central part of the Western Siberia (55-62ºN; 64-88ºE) and the Tomsk region (56-61ºN; 75-88ºE) are highlighted by boxes.

Atmos. Meas. Tech. Discuss., doi:10.5194/amt-2016-244, 2016
Manuscript under review for journal Atmos. Meas. Tech.
Published: 15 August 2016

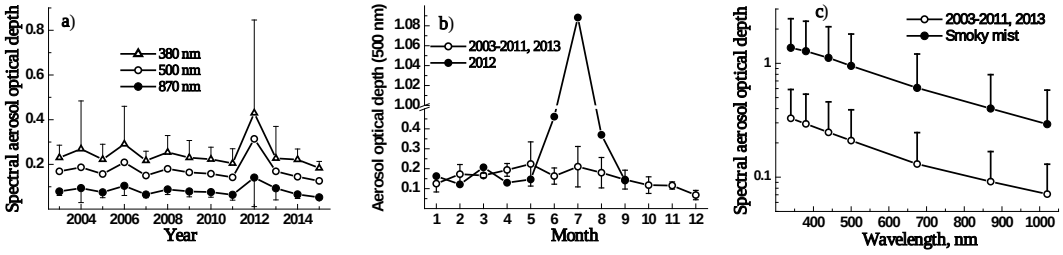

Figure 6. (a) Multiyear averages of spectral aerosol optical depth; (b) monthly averages of τ_{500} in 2012 compared with the multiyear averages for the period of 2003-2011, 2013; and (c) average spectral AOD dependences in the period of smoke mist as compared to multiyear data in July (Tomsk, 2003-2011, 2013, combined dataset of smoke and background situations)

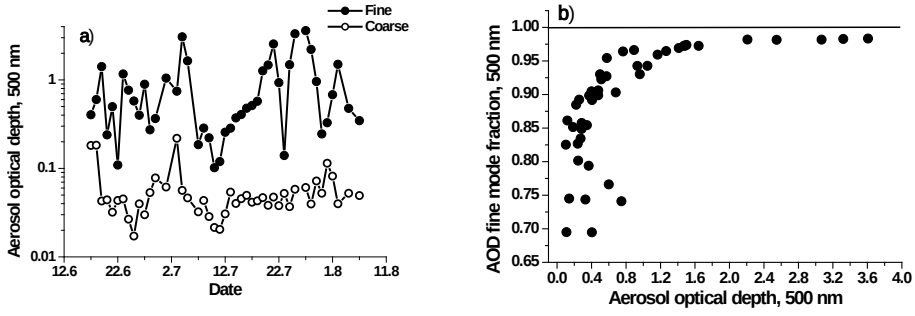

Figure 7. (a) Time series of computed average fine and coarse AOD mode; (b) fine mode fraction of AOD as a function of AOD (500 nm) for the Tomsk data during smoke mist in 2012

Atmos. Meas. Tech. Discuss., doi:10.5194/amt-2016-244, 2016
Manuscript under review for journal Atmos. Meas. Tech.
Published: 15 August 2016

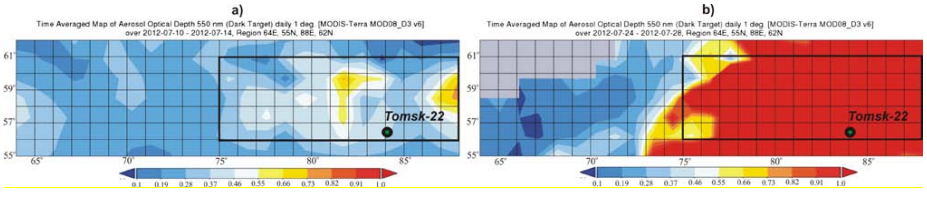

Figure 8. Spatial AOD distribution over the central part of the Western Siberia according to MODIS data for summer 2012: a) July 10-14, b) July 24-28.

Atmos. Meas. Tech. Discuss., doi:10.5194/amt-2016-244, 2016
Manuscript under review for journal Atmos. Meas. Tech.
Published: 15 August 2016

Atmospheric Measurement Techniques Discussions

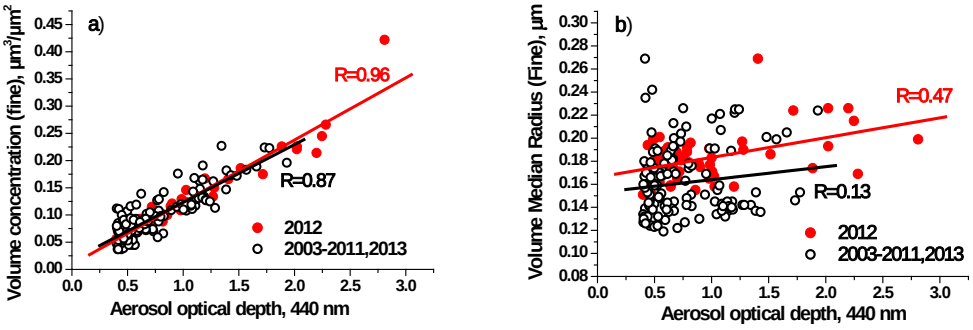

Figure 9. (a) Fine mode volume concentration and (b) median radius versus AOD(440 nm) in Tomsk.

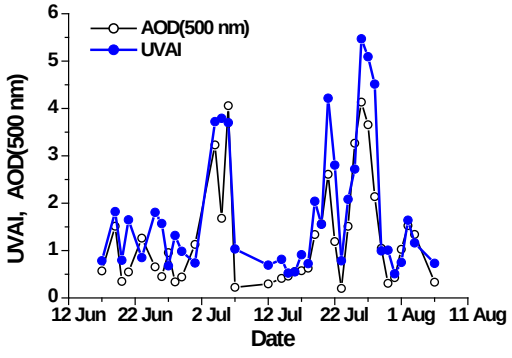

Figure 10. Ultraviolet Aerosol Index (http://giovanni.sci.gsfc.nasa.gov/giovanni/) near Tomsk (55-57°N, 83-85°E) and AOD according to data of ground-based measurements (http://aeronet.gsfc.nasa.gov)

Atmos. Meas. Tech. Discuss., doi:10.5194/amt-2016-244, 2016
Manuscript under review for journal Atmos. Meas. Tech.
Published: 15 August 2016

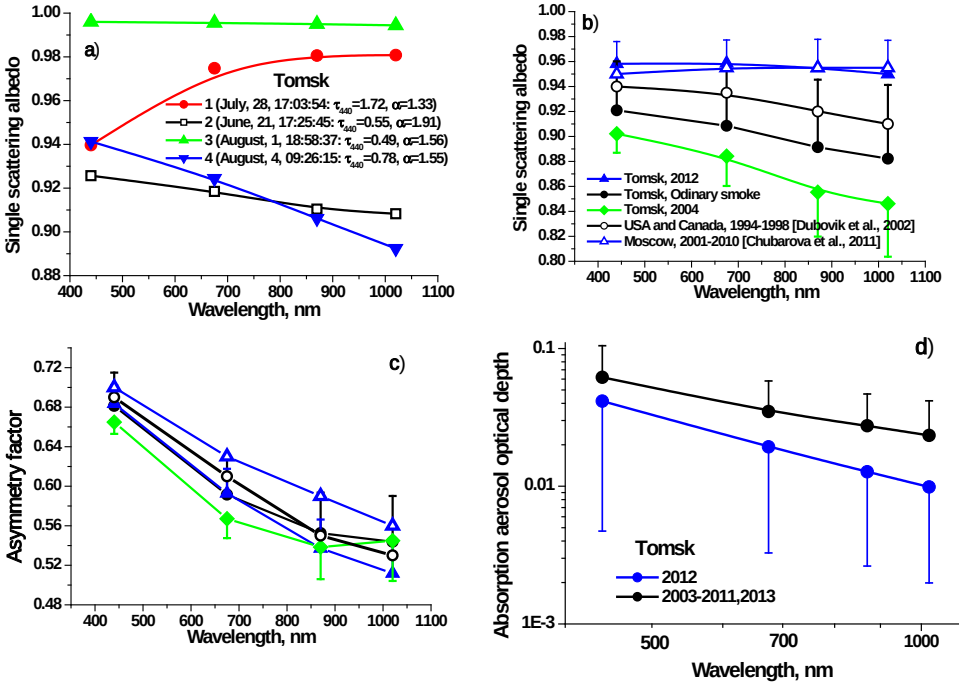

Figure 11. (a) Examples of spectral dependence of SSA; averaged (b) SSA and (c) AF for different periods and regions of observations; and (d) average spectral absorption aerosol optical depth for 2012 smoke mist and "ordinary" smokes.

Atmos. Meas. Tech. Discuss., doi:10.5194/amt-2016-244, 2016
Manuscript under review for journal Atmos. Meas. Tech.
Published: 15 August 2016

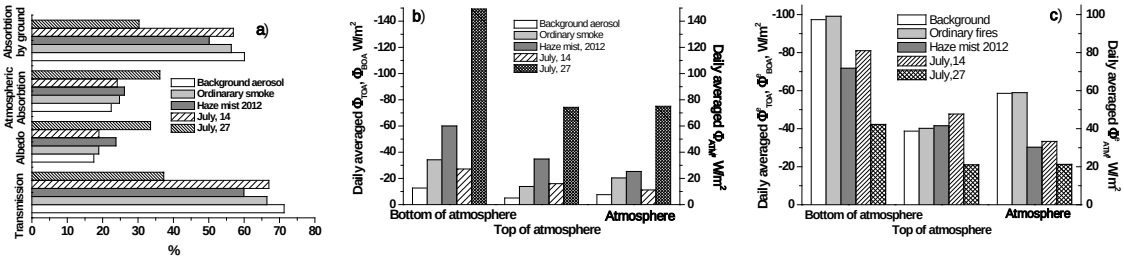

Figure 12. Radiative effects of aerosol under different atmospheric conditions.